

Triply charm and bottom tetraquarks in a constituent quark model

Gang Yang,^{1,*} Jialun Ping,^{2,†} and Jorge Segovia^{3,‡}

¹*Department of Physics, Zhejiang Normal University, Jinhua 321004, China*

²*Department of Physics and Jiangsu Key Laboratory for Numerical Simulation of Large Scale Complex Systems, Nanjing Normal University, Nanjing 210023, P. R. China*

³*Departamento de Sistemas Físicos, Químicos y Naturales, Universidad Pablo de Olavide, E-41013 Sevilla, Spain*

Singly, doubly and fully charmed tetraquark candidates, *e.g.*, $T_{c\bar{s}}(2900)$, $T_{cc}^+(3875)$ and $X(6900)$ have been recently reported by the LHCb collaboration. Therefore, it is timely to implement a theoretical investigation on triply heavy tetraquark systems; herein, the S-wave triply charm and bottom tetraquarks, $\bar{Q}Q\bar{q}Q$ ($q = u, d, s$; $Q = c, b$), with spin-parity $J^P = 0^+, 1^+$ and 2^+ , isospin $I = 0$ and $\frac{1}{2}$, are systematically studied in a constituent quark model. Besides, all tetraquark configurations, *i.e.* meson-meson, diquark-antidiquark and K-type arrangements, along with any allowed color structure, are comprehensively considered. The Gaussian expansion method (GEM), in combination with the complex-scaling method (CSM), which is quite ingenious in dealing with either bound or resonances, is the approach adopted in solving the complex scaled Schrödinger equation. This theoretical framework has already been applied in various tetra- and penta-quark systems. In a fully coupled-channel calculation within the GEM+CSM, narrow resonances are found in each $I(J^P)$ channel of the charm and bottom sector. In particular, triply charm and bottom tetraquark resonances are obtained in 5.6 – 5.9 GeV and 15.3 – 15.7 GeV, respectively. We provide also some insights of the compositeness of these exotic states, such as the inner quark distance, magnetic moment and dominant wave function component. All this may help to distinguish them in future high energy nuclear and particle experiments.

I. INTRODUCTION

In the past two decades, a large amount of crucial findings on exotic hadrons in heavy flavor sectors have been reported experimentally. In particular, tetraquark candidates in the charm-strange sector, $X_{0,(1)}(2900)$ and $T_{c\bar{s}}^{0(++)}(2900)$ were reported by the LHCb collaboration in studying B meson three-body strong decays [1–4]. In 2021, a double charm tetraquark candidate, $T_{cc}^+(3875)$, which is quite close to the $D^{*+}D^0$ threshold, was announced by the same collaboration [5, 6]. Moreover, in the fully charmed sector, four exotic states, which are denoted as $X(6400)$, $X(6600)$, $X(6900)$ and $X(7200)$, were reported by the LHCb, CMS and ATLAS collaborations [7–9]. At the same time, an enormous theoretical effort with a wide variety of approaches has been carried out in order to reveal the nature of exotic hadrons. Generally, there are extensive reviews [10–29], which explain in detail a particular theoretical method and thus capture a certain interpretation of exotic states.

One can realize from above that singly, doubly and fully heavy tetraquarks have been observed experimentally and thus asking oneself if there are tetraquarks with three constituent heavy quarks. Until now, there is no experimental data on triply heavy tetraquarks. Besides, no bound states of $QQ\bar{Q}\bar{q}$ tetraquark system are obtained in several studies using the MIT bag model [30], an effective field theory approach [31], the extended chromomag-

netic model [32], the relativized quark model [33], and QCD sum rules [34]. In contrast, several bound states are obtained in the $cc\bar{c}\bar{q}$ tetraquark system using a chiral quark model [35]. Furthermore, it is found that some $bb\bar{b}\bar{q}$ tetraquark states may lie below the bottomonia plus $B^{(*)}$ thresholds [34]. Moreover, stable excited states of triply heavy tetraquarks are also found [30, 34, 36–38], calculating, besides their masses, magnetic moments, charge radii and decay properties.

We perform a systematic investigation on triply heavy tetraquarks, $\bar{Q}Q\bar{q}Q$ ($q = u, d, s$; $Q = c, b$), in a constituent quark model. This approach has been already applied with reasonable success in predictions and descriptions of various tetra- and penta-quark systems, *e.g.*, hidden-, single- double- and fully-heavy tetraquarks [39–46], and pentaquarks [47–51]. The wave functions of S-wave $\bar{Q}Q\bar{q}Q$ tetraquarks, with spin-parity $J^P = 0^+, 1^+$ and 2^+ , isospin $I = 0$ and $\frac{1}{2}$, are comprehensively constructed by including meson-meson, diquark-antidiquark and K-type arrangements of quarks, along with all allowed color structures. A high accuracy and efficient numerical approach, the Gaussian expansion method (GEM) [52], along with a powerful complex scaling method (CSM), which is quite ingenious in dealing with bound and resonant states simultaneously, is employed to solve the resulting Schrödinger equation for the four-body system.

This article is arranged as follows. In Sec. II the theoretical framework is presented, it includes a detailed explanation of the constituent quark model and wave functions of the $\bar{Q}Q\bar{q}Q$ tetraquarks. Section III is devoted to the analysis of the calculated results. Finally, a summary can be found in Sec. IV.

* yanggang@zjnu.edu.cn

† jlping@njnu.edu.cn

‡ jsegovia@upo.es

II. THEORETICAL FRAMEWORK

The theoretical formalism employed herein has been previously published in Ref. [15], and we shall then focus on the most relevant features of the model and the numerical approach concerning the $QQ\bar{q}Q$ tetraquarks.

A. The Hamiltonian

We solve the complex-scaled Schrödinger equation to study the 4-body bound and resonant states, the equation is

$$[H(\theta) - E(\theta)] \Psi_{JM}(\theta) = 0, \quad (1)$$

with $E(\theta)$ and $\Psi(\theta)$ the eigenenergies and eigenfunctions, respectively, and the 4-body Hamiltonian for a QCD-inspired constituent quark model reads as

$$H(\theta) = \sum_{i=1}^4 \left(m_i + \frac{(\vec{p}_i e^{-i\theta})^2}{2m_i} \right) - T_{\text{CM}} + \sum_{j>i=1}^4 V(\vec{r}_{ij} e^{i\theta}), \quad (2)$$

where m_i is the constituent quark mass, \vec{p}_i is the momentum of a quark, T_{CM} is the center-of-mass kinetic energy and the last term is the two-body potential.

By introducing an artificial parameter, *i.e.* the rotated angle θ , three kinds of complex eigenvalues: bound, resonance and scattering states, can be simultaneously studied. Particularly, bound and resonance states are independent of the rotated angle θ , with the first ones always placed on the real-axis of the complex energy plane, and the second ones located above the threshold line with a total decay width $\Gamma = -2\text{Im}(E)$. Meanwhile, the scattering state are unstable with respect the rotated angle θ and align along the corresponding threshold line.

The dynamics of triply charm and bottom tetraquark systems are driven by two-body complex-scaled potentials,

$$V(\vec{r}_{ij} e^{i\theta}) = V_{\text{CON}}(\vec{r}_{ij} e^{i\theta}) + V_{\text{OGE}}(\vec{r}_{ij} e^{i\theta}). \quad (3)$$

In particular, color-confinement and perturbative one-gluon exchange interactions are the most relevant features of QCD in its low energy regime since the presence of heavy quarks make chiral symmetry explicitly broken. Since the lowest-lying S -wave positive parity triply heavy tetraquarks shall be investigated, only central and spin-spin terms of the interactions are considered.

Color confinement should be encoded in the non-Abelian character of QCD. On one hand, lattice-regularized QCD has demonstrated that multi-gluon exchanges produce an attractive linearly rising potential proportional to the distance between infinite-heavy quarks [53]. On the other hand, the spontaneous creation of light-quark pairs from the QCD vacuum may give rise at the same scale to a breakup of the created color flux-tube [53]. We can phenomenologically describe the above

TABLE I. Quark model parameters.

Quark masses	m_q ($q = u, d$) (MeV)	313
	m_s (MeV)	555
	m_c (MeV)	1752
	m_b (MeV)	5100
Confinement	a_c (MeV)	430
	μ_c (fm^{-1})	0.70
	Δ (MeV)	181.10
OGE	α_0	2.118
	Λ_0 (fm^{-1})	0.113
	μ_0 (MeV)	36.976
	\hat{r}_0 (MeV fm)	28.17

two observations by implementing the following confining effective potential [54, 55]

$$V_{\text{CON}}(\vec{r}_{ij} e^{i\theta}) = \left[-a_c(1 - e^{-\mu_c r_{ij} e^{i\theta}}) + \Delta \right] (\lambda_i^c \cdot \lambda_j^c), \quad (4)$$

where λ^c denote the SU(3) color Gell-Mann matrices, whereas a_c , μ_c and Δ are model parameters. When the rotated angle θ is 0° , one can see in Eq. (4) that the real-range potential is linear at short inter-quark distances with an effective confinement strength $\sigma = -a_c \mu_c (\lambda_i^c \cdot \lambda_j^c)$, while it becomes a constant at large distances, $V_{\text{thr.}} = (\Delta - a_c)(\lambda_i^c \cdot \lambda_j^c)$.

The perturbative one-gluon exchange potential, which includes the so-called Coulomb and color-magnetic interactions, is [54, 55]

$$V_{\text{OGE}}(\vec{r}_{ij} e^{i\theta}) = \frac{1}{4} \alpha_s (\lambda_i^c \cdot \lambda_j^c) \left[\frac{1}{r_{ij} e^{i\theta}} - \frac{1}{6m_i m_j} (\vec{\sigma}_i \cdot \vec{\sigma}_j) \frac{e^{-r_{ij} e^{i\theta}/r_0(\mu_{ij})}}{r_{ij} e^{i\theta} r_0^2(\mu_{ij})} \right], \quad (5)$$

where $\vec{\sigma}$ denote the Pauli matrices and the regularized contact term is given by

$$\delta(\vec{r}_{ij} e^{i\theta}) \sim \frac{1}{4\pi r_0^2(\mu_{ij})} \frac{e^{-r_{ij} e^{i\theta}/r_0(\mu_{ij})}}{r_{ij} e^{i\theta}}. \quad (6)$$

with $r_0(\mu_{ij}) = \hat{r}_0/\mu_{ij}$ a regulator that depends on the reduced mass of the quark-(anti-)quark pair.

An effective scale-dependent strong coupling constant provides a consistent description of mesons and baryons from light to heavy quark sectors. Its effective parametrization has the expression [54, 55]

$$\alpha_s(\mu_{ij}) = \frac{\alpha_0}{\ln\left(\frac{\mu_{ij}^2 + \mu_0^2}{\Lambda_0^2}\right)}, \quad (7)$$

where α_0 , μ_0 and Λ_0 are model parameters.

TABLE II. Theoretical and experimental (if available) masses of $1S$ and $2S$ states of $Q\bar{Q}$ and $Q\bar{q}$ ($q = u, d, s$; $Q = c, b$) mesons, unit in MeV.

Meson	nL	$M_{\text{The.}}$	$M_{\text{Exp.}}$	Meson	nL	$M_{\text{The.}}$	$M_{\text{Exp.}}$
η_c	$1S$	2989	2981	η_b	$1S$	9454	9300
	$2S$	3627	—		$2S$	9985	—
J/ψ	$1S$	3097	3097	Υ	$1S$	9505	9460
	$2S$	3685	—		$2S$	10013	10023
D	$1S$	1897	1870	B	$1S$	5278	5280
	$2S$	2648	—		$2S$	5984	—
D^*	$1S$	2017	2007	B^*	$1S$	5319	5325
	$2S$	2704	—		$2S$	6005	—
D_s	$1S$	1989	1968	B_s	$1S$	5355	5367
	$2S$	2705	—		$2S$	6017	—
D_s^*	$1S$	2115	2112	B_s^*	$1S$	5400	5415
	$2S$	2769	—		$2S$	6042	—

All discussed model parameters are summarized in Table I. They have been fixed attending the phenomenology of conventional heavy hadrons, studying their spectra [56–59], their electromagnetic, weak and strong decays and reactions [60–63], as well as the coupling between naive meson states and meson-meson thresholds [64–67]; see also reviews [23, 68] to infer its application to meson-meson, baryon-meson and baryon-baryon states. Furthermore, for later concern, Table II lists theoretical and experimental (if available) masses of ground and first excited states of $Q\bar{Q}$ and $Q\bar{q}$ ($q = u, d, s$; $Q = c, b$) mesons.

B. The wave function

The $\bar{Q}Q\bar{q}Q$ ($q = u, d, s$; $Q = c, b$) tetraquark configurations, which are under investigation in this work, are presented in Figure 1. Particularly, Fig. 1(a) is the meson-meson structure, Fig. 1(b) is the diquark-antidiquark arrangement, and panels (c) to (g) of Fig. 1 are the five K-type configurations, which are rarely referred in other studies on multi-quark systems.

The total wave function of a tetraquark system at the quark level is an internal product of color, spin, flavor and space wave functions. Concerning the color degree-of-freedom, the colorless wave function of a 4-quark system in meson-meson configuration can be obtained by either two coupled color-singlet clusters, $1 \otimes 1$:

$$\chi_1^c = \frac{1}{3}(\bar{r}r + \bar{g}g + \bar{b}b) \times (\bar{r}r + \bar{g}g + \bar{b}b), \quad (8)$$

or two coupled color-octet clusters, $8 \otimes 8$:

$$\begin{aligned} \chi_2^c = & \frac{\sqrt{2}}{12}(3\bar{b}r\bar{r}b + 3\bar{g}r\bar{r}g + 3\bar{b}g\bar{g}b + 3\bar{g}b\bar{b}g + 3\bar{r}g\bar{g}r \\ & + 3\bar{r}b\bar{b}r + 2\bar{r}r\bar{r}r + 2\bar{g}g\bar{g}g + 2\bar{b}b\bar{b}b - \bar{r}r\bar{g}g \\ & - \bar{g}g\bar{r}r - \bar{b}b\bar{g}g - \bar{b}b\bar{r}r - \bar{g}g\bar{b}b - \bar{r}r\bar{b}b). \end{aligned} \quad (9)$$

For future reference, note herein that the first color state is the so-called color-singlet channel and the second one is the named hidden-color case.

The color wave functions associated to the diquark-antidiquark structure are the coupled color triplet-antitriplet clusters, $3 \otimes \bar{3}$:

$$\begin{aligned} \chi_3^c = & \frac{\sqrt{3}}{6}(\bar{r}r\bar{g}g - \bar{g}r\bar{r}g + \bar{g}g\bar{r}r - \bar{r}g\bar{g}r + \bar{r}r\bar{b}b \\ & - \bar{b}r\bar{r}b + \bar{b}b\bar{r}r - \bar{r}b\bar{b}r + \bar{g}g\bar{b}b - \bar{b}g\bar{g}b \\ & + \bar{b}b\bar{g}g - \bar{g}b\bar{b}g), \end{aligned} \quad (10)$$

and the coupled color sextet-antisextet clusters, $6 \otimes \bar{6}$:

$$\begin{aligned} \chi_4^c = & \frac{\sqrt{6}}{12}(2\bar{r}r\bar{r}r + 2\bar{g}g\bar{g}g + 2\bar{b}b\bar{b}b + \bar{r}r\bar{g}g + \bar{g}r\bar{r}g \\ & + \bar{g}g\bar{r}r + \bar{r}g\bar{g}r + \bar{r}r\bar{b}b + \bar{b}r\bar{r}b + \bar{b}b\bar{r}r \\ & + \bar{r}b\bar{b}r + \bar{g}g\bar{b}b + \bar{b}g\bar{g}b + \bar{b}b\bar{g}g + \bar{g}b\bar{b}g). \end{aligned} \quad (11)$$

Meanwhile, the possible color-singlet wave functions obtained from the five K-type configurations are

$$\begin{aligned} \chi_5^c = & \frac{1}{6\sqrt{2}}(\bar{r}r\bar{r}r + \bar{g}g\bar{g}g - 2\bar{b}b\bar{b}b) + \\ & \frac{1}{2\sqrt{2}}(\bar{r}b\bar{b}r + \bar{r}g\bar{g}r + \bar{g}b\bar{b}g + \bar{g}r\bar{r}g + \bar{b}g\bar{g}b + \bar{b}r\bar{r}b) - \\ & \frac{1}{3\sqrt{2}}(\bar{g}g\bar{r}r + \bar{r}r\bar{g}g) + \frac{1}{6\sqrt{2}}(\bar{b}b\bar{r}r + \bar{b}b\bar{g}g + \bar{r}r\bar{b}b + \bar{g}g\bar{b}b), \end{aligned} \quad (12)$$

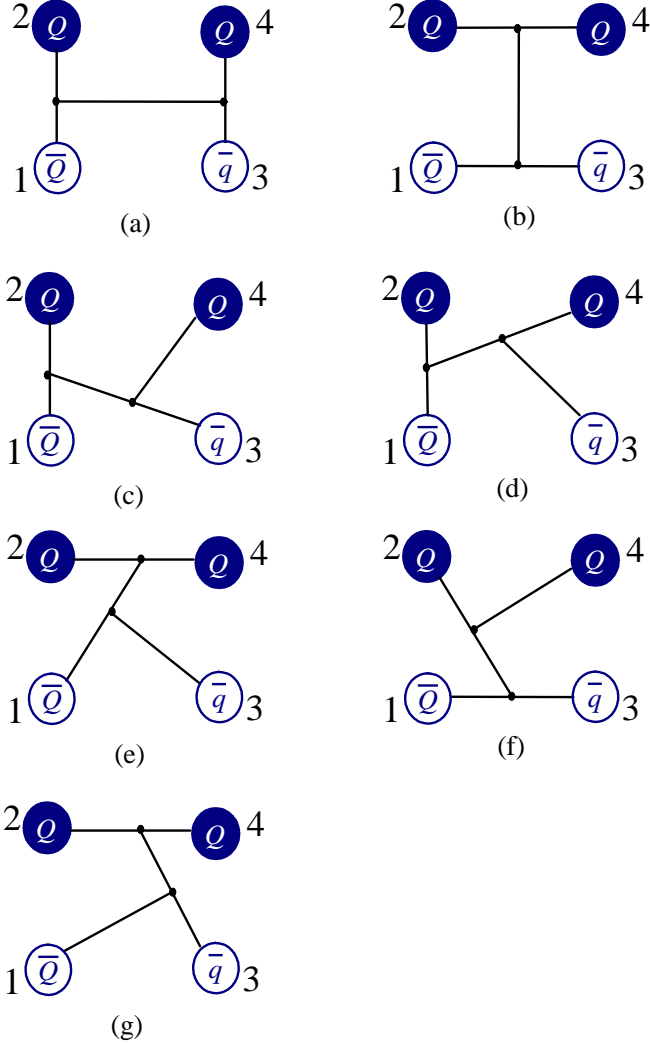


FIG. 1. Possible configurations of triply heavy tetraquarks $\bar{Q}Q\bar{q}Q$ ($q = u, d, s$; $Q = c, b$). In particular, panel (a) is meson-meson structure, panel (b) is diquark-antidiquark arrangement, and the five K-type configurations are from panel (c) to (g).

$$\chi_6^c = \chi_1^c, \quad (13)$$

$$\chi_7^c = \chi_1^c, \quad (14)$$

$$\chi_8^c = \chi_2^c, \quad (15)$$

$$\begin{aligned} \chi_9^c = & \frac{1}{2\sqrt{6}}(\bar{r}b\bar{b}r + \bar{r}r\bar{b}b + \bar{g}b\bar{b}g + \bar{g}g\bar{b}b + \bar{r}g\bar{g}r + \bar{r}r\bar{g}g + \\ & \bar{b}b\bar{g}g + \bar{b}g\bar{g}b + \bar{g}g\bar{r}r + \bar{g}r\bar{r}g + \bar{b}b\bar{r}r + \bar{b}r\bar{r}b) + \\ & \frac{1}{\sqrt{6}}(\bar{r}r\bar{r}r + \bar{g}g\bar{g}g + \bar{b}b\bar{b}b), \end{aligned} \quad (16)$$

$$\begin{aligned} \chi_{10}^c = & \frac{1}{2\sqrt{3}}(\bar{r}b\bar{b}r - \bar{r}r\bar{b}b + \bar{g}b\bar{b}g - \bar{g}g\bar{b}b + \bar{r}g\bar{g}r - \bar{r}r\bar{g}g - \\ & \bar{b}b\bar{g}g + \bar{b}g\bar{g}b - \bar{g}g\bar{r}r + \bar{g}r\bar{r}g - \bar{b}b\bar{r}r + \bar{b}r\bar{r}b), \end{aligned} \quad (17)$$

$$\chi_{11}^c = \chi_9^c, \quad (18)$$

$$\chi_{12}^c = -\chi_{10}^c. \quad (19)$$

$$\chi_{13}^c = \chi_9^c, \quad (20)$$

$$\chi_{14}^c = \chi_{10}^c. \quad (21)$$

Let us now consider the spin wave functions, $\chi_{S, M_S}^{\sigma_i}$, for S -wave ground states with spin (S) ranging from 0 to 2 (M_S can be set to be equal to S without loss of generality). For $(S, M_S) = (0, 0)$, one has

$$\chi_{0,0}^{\sigma_{u_1}}(4) = \chi_{00}^{\sigma}\chi_{00}^{\sigma}, \quad (22)$$

$$\chi_{0,0}^{\sigma_{u_2}}(4) = \frac{1}{\sqrt{3}}(\chi_{11}^{\sigma}\chi_{1,-1}^{\sigma} - \chi_{10}^{\sigma}\chi_{10}^{\sigma} + \chi_{1,-1}^{\sigma}\chi_{11}^{\sigma}), \quad (23)$$

$$\begin{aligned} \chi_{0,0}^{\sigma_{u_3}}(4) = & \frac{1}{\sqrt{2}}((\sqrt{\frac{2}{3}}\chi_{11}^{\sigma}\chi_{\frac{1}{2},-\frac{1}{2}}^{\sigma} - \sqrt{\frac{1}{3}}\chi_{10}^{\sigma}\chi_{\frac{1}{2},\frac{1}{2}}^{\sigma})\chi_{\frac{1}{2},-\frac{1}{2}}^{\sigma} \\ & - (\sqrt{\frac{1}{3}}\chi_{10}^{\sigma}\chi_{\frac{1}{2},-\frac{1}{2}}^{\sigma} - \sqrt{\frac{2}{3}}\chi_{1,-1}^{\sigma}\chi_{\frac{1}{2},\frac{1}{2}}^{\sigma})\chi_{\frac{1}{2},\frac{1}{2}}^{\sigma}), \end{aligned} \quad (24)$$

$$\chi_{0,0}^{\sigma_{u_4}}(4) = \frac{1}{\sqrt{2}}(\chi_{00}^{\sigma}\chi_{\frac{1}{2},\frac{1}{2}}^{\sigma}\chi_{\frac{1}{2},-\frac{1}{2}}^{\sigma} - \chi_{00}^{\sigma}\chi_{\frac{1}{2},-\frac{1}{2}}^{\sigma}\chi_{\frac{1}{2},\frac{1}{2}}^{\sigma}), \quad (25)$$

for $(S, M_S) = (1, 1)$, the spin wave functions are

$$\chi_{1,1}^{\sigma_{w_1}}(4) = \chi_{00}^{\sigma}\chi_{11}^{\sigma}, \quad (26)$$

$$\chi_{1,1}^{\sigma_{w_2}}(4) = \chi_{11}^{\sigma}\chi_{00}^{\sigma}, \quad (27)$$

$$\chi_{1,1}^{\sigma_{w_3}}(4) = \frac{1}{\sqrt{2}}(\chi_{11}^{\sigma}\chi_{10}^{\sigma} - \chi_{10}^{\sigma}\chi_{11}^{\sigma}), \quad (28)$$

$$\begin{aligned} \chi_{1,1}^{\sigma_{w_4}}(4) = & \sqrt{\frac{3}{4}}\chi_{11}^{\sigma}\chi_{\frac{1}{2},\frac{1}{2}}^{\sigma}\chi_{\frac{1}{2},-\frac{1}{2}}^{\sigma} - \sqrt{\frac{1}{12}}\chi_{11}^{\sigma}\chi_{\frac{1}{2},-\frac{1}{2}}^{\sigma}\chi_{\frac{1}{2},\frac{1}{2}}^{\sigma} \\ & - \sqrt{\frac{1}{6}}\chi_{10}^{\sigma}\chi_{\frac{1}{2},\frac{1}{2}}^{\sigma}\chi_{\frac{1}{2},\frac{1}{2}}^{\sigma}, \end{aligned} \quad (29)$$

$$\chi_{1,1}^{\sigma_{w_5}}(4) = (\sqrt{\frac{2}{3}}\chi_{11}^{\sigma}\chi_{\frac{1}{2},-\frac{1}{2}}^{\sigma} - \sqrt{\frac{1}{3}}\chi_{10}^{\sigma}\chi_{\frac{1}{2},\frac{1}{2}}^{\sigma})\chi_{\frac{1}{2},\frac{1}{2}}^{\sigma}, \quad (30)$$

$$\chi_{1,1}^{\sigma_{w_6}}(4) = \chi_{00}^{\sigma}\chi_{\frac{1}{2},\frac{1}{2}}^{\sigma}\chi_{\frac{1}{2},\frac{1}{2}}^{\sigma}, \quad (31)$$

and, for $(S, M_S) = (2, 2)$, one has

$$\chi_{2,2}^{\sigma_1}(4) = \chi_{11}^{\sigma}\chi_{11}^{\sigma}. \quad (32)$$

Besides, the superscripts u_1, \dots, u_4 and w_1, \dots, w_6 determine the spin wave function for each configuration of tetraquark system, their values are listed in Table III. Furthermore, the expressions above are obtained by considering the coupling between two sub-clusters whose spin wave functions are given by trivial SU(2) algebra, whose basis reads as

$$\chi_{00}^{\sigma} = \frac{1}{\sqrt{2}}(\chi_{\frac{1}{2},\frac{1}{2}}^{\sigma}\chi_{\frac{1}{2},-\frac{1}{2}}^{\sigma} - \chi_{\frac{1}{2},-\frac{1}{2}}^{\sigma}\chi_{\frac{1}{2},\frac{1}{2}}^{\sigma}), \quad (33)$$

$$\chi_{11}^{\sigma} = \chi_{\frac{1}{2},\frac{1}{2}}^{\sigma}\chi_{\frac{1}{2},\frac{1}{2}}^{\sigma}, \quad (34)$$

$$\chi_{1,-1}^{\sigma} = \chi_{\frac{1}{2},-\frac{1}{2}}^{\sigma}\chi_{\frac{1}{2},-\frac{1}{2}}^{\sigma}, \quad (35)$$

$$\chi_{10}^{\sigma} = \frac{1}{\sqrt{2}}(\chi_{\frac{1}{2},\frac{1}{2}}^{\sigma}\chi_{\frac{1}{2},-\frac{1}{2}}^{\sigma} + \chi_{\frac{1}{2},-\frac{1}{2}}^{\sigma}\chi_{\frac{1}{2},\frac{1}{2}}^{\sigma}). \quad (36)$$

TABLE III. The values of the superscripts u_1, \dots, u_4 and w_1, \dots, w_6 that determine the spin wave function for each configuration of the triply heavy tetraquark systems.

	Di-meson	Diquark-antidiquark	K_1	K_2	K_3	K_4	K_5
u_1	1	3					
u_2	2	4					
u_3			5	7	9	11	13
u_4			6	8	10	12	14
w_1	1	4					
w_2	2	5					
w_3	3	6					
w_4			7	10	13	16	19
w_5			8	11	14	17	20
w_6			9	12	15	18	21

The flavor wave functions, χ_I^f , of triply charm and bottom tetraquarks are simply denoted as

$$\chi_I^f = \bar{Q}Q\bar{q}Q, \quad (q = u, d, s; Q = c, b), \quad (37)$$

where the isospin, I , and its third component, M_I , are both equal to zero for the $\bar{Q}Q\bar{s}Q$ system, while they are $\frac{1}{2}$ for the $\bar{Q}Q\bar{d}Q$ one.

We use the Rayleigh-Ritz variational principle to solve the Schrödinger-like four-body equation. Within a complex-scaled theoretical framework, the spatial wave function reads as below:

$$\psi_{LM_L} = \left[\left[\phi_{n_1 l_1}(\vec{\rho} e^{i\theta}) \phi_{n_2 l_2}(\vec{\lambda} e^{i\theta}) \right]_l \phi_{n_3 l_3}(\vec{R} e^{i\theta}) \right]_{LM_L}, \quad (38)$$

where the internal Jacobi coordinates are defined as

$$\vec{\rho} = \vec{x}_1 - \vec{x}_{2(4)}, \quad (39)$$

$$\vec{\lambda} = \vec{x}_3 - \vec{x}_{4(2)}, \quad (40)$$

$$\vec{R} = \frac{m_1 \vec{x}_1 + m_{2(4)} \vec{x}_{2(4)}}{m_1 + m_{2(4)}} - \frac{m_3 \vec{x}_3 + m_{4(2)} \vec{x}_{4(2)}}{m_3 + m_{4(2)}}, \quad (41)$$

for the meson-meson configuration of Fig. 1(a), and as

$$\vec{\rho} = \vec{x}_1 - \vec{x}_3, \quad (42)$$

$$\vec{\lambda} = \vec{x}_2 - \vec{x}_4, \quad (43)$$

$$\vec{R} = \frac{m_1 \vec{x}_1 + m_3 \vec{x}_3}{m_1 + m_3} - \frac{m_2 \vec{x}_2 + m_4 \vec{x}_4}{m_2 + m_4}, \quad (44)$$

for the diquark-antidiquark arrangement of Fig. 1(b). The remaining five K-type configurations shown in panels (c) to (g) of Fig. 1 are (i, j, k, l) take values according to the panels (c) to (g) of Fig. 1):

$$\vec{\rho} = \vec{x}_i - \vec{x}_j, \quad (45)$$

$$\vec{\lambda} = \vec{x}_k - \frac{m_i \vec{x}_i + m_j \vec{x}_j}{m_i + m_j}, \quad (46)$$

$$\vec{R} = \vec{x}_l - \frac{m_i \vec{x}_i + m_j \vec{x}_j + m_k \vec{x}_k}{m_i + m_j + m_k}. \quad (47)$$

Obviously, the center-of-mass kinetic term, T_{CM} , can be completely eliminated for a non-relativistic system defined in any of the above sets of relative motion coordinates.

The basis expansion of the space wave function of Eq. (38) is performed by employing the Gaussian expansion method (GEM) [52], which has been proven to be quite efficient on solving bound- and scattering-state problems of a few- and many-body systems. This consists basically on using Gaussian basis functions, whose sizes are taken in geometric progression, for each relative motion of the tetraquark system (see Ref. [47] for details). Hence, the form of the orbital wave function ϕ_{nlm} in Eq. (38) is simply

$$\phi_{nlm}(\vec{r} e^{i\theta}) = \sqrt{1/4\pi} N_{nl} (r e^{i\theta})^l e^{-\nu_n (r e^{i\theta})^2}. \quad (48)$$

Finally, the complete wave function, which fulfills the Pauli principle, is written as

$$\begin{aligned} \Psi_{JM_J, I} &= \sum_{i,j} c_{ij} \Psi_{JM_J, I, i, j} \\ &= \sum_{i,j} c_{ij} \mathcal{A} \left[[\psi_{LM_L} \chi_{SM_S}^{\sigma_i} (4)]_{JM_J} \chi_I^f \chi_j^c \right], \end{aligned} \quad (49)$$

where \mathcal{A} is the antisymmetry operator of $\bar{Q}Q\bar{q}Q$ tetraquark systems, which take into account the fact of involving two identical heavy quarks. Its definition, according to Fig. 1, is

$$\mathcal{A} = 1 - (24). \quad (50)$$

This is necessary in our theoretical framework, since the complete wave function of the 4-quark system is constructed from two sub-clusters: meson-meson, diquark-antidiquark and K-type configurations.

Since our intention is to shed some light about the nature of triply heavy tetraquarks, their internal structure is studied by quantitative analyses of the inter-quark distance,

$$r_{q\bar{q}} = \text{Re}(\sqrt{\langle \Psi_{JM_J, I} | (r_{q\bar{q}} e^{i\theta})^2 | \Psi_{JM_J, I} \rangle}), \quad (51)$$

and magnetic moment,

$$\mu_m = \text{Re}(\langle \Psi_{JM_J, I} | \sum_{i=1}^4 \frac{\hat{Q}_i}{2m_i} \hat{\sigma}_i^z | \Psi_{JM_J, I} \rangle). \quad (52)$$

Moreover, a qualitative survey of the dominant configuration or component,

$$C_p = \text{Re}(\sum_{i,j} \langle c_{ij}^l \Psi_{JM_J, I, i, j} | c_{ij}^r \Psi_{JM_J, I, i, j} \rangle), \quad (53)$$

is also performed. Meanwhile, in Eq. (52), \hat{Q}_i is the electric charge operator of the i -th quark and σ_i^z is the z -component of Pauli matrix. Moreover, c_{ij}^l and c_{ij}^r denote, respectively, the left and right generalized eigenvectors of

the complete anti-symmetric complex wave function. Finally, note that these observables are complex numbers in the complex scaling method, and thus their real-parts are analyzed for that resonance whose width is small where the approach is expected to work well.

One inevitable issue of our theoretical framework has to be pointed. The different multi-quark channels are not orthogonal to each other. Accordingly, we perform two kinds of computations related with the triply heavy tetraquarks components. Consider an n -dimension matrix representation of the overlap in Eq. (53):

$$\begin{pmatrix} c_{11} & c_{12} & \cdots & c_{1n} \\ c_{21} & c_{22} & \cdots & c_{2n} \\ \vdots & \vdots & \ddots & \vdots \\ c_{n1} & c_{n2} & \cdots & c_{nn} \end{pmatrix}.$$

One can firstly consider the diagonal elements only in obtaining the relative weights of each channel or, secondly, the off-diagonal elements are employed by adding all such elements in the i -th row to the i -th diagonal element. A comparison on these two ways of proceed help us significantly in identifying the dominant component of the exotic state, and to express some conclusions about the off-diagonal contributions.

III. RESULTS

We proceed to discuss our results on $\bar{Q}Q\bar{q}Q$ ($q = u, d, s$; $Q = c, b$) tetraquarks, considering all possible meson-meson, diquark-antidiquark and K-type arrangements. Since we are interested on S -wave states, the total angular momentum, J , coincides with the total spin, S , and can take values of 0, 1 and 2, respectively. The systems' isospin is $\frac{1}{2}$ for $\bar{Q}Q\bar{d}Q$ and 0 for $\bar{Q}Q\bar{s}Q$. With the purpose of solving a manageable problem of eigen-values and -vectors, the artificial parameter of rotated angle is ranged from 0° to 6° ; being the rotated angle $\theta = 0^\circ$ the real-range case and the rest used to distinguish between bound, resonance and scattering states in the complex energy plane.

Tables IV to XXVIII list calculated results of $\bar{Q}Q\bar{q}Q$ tetraquark states. In particular, real-range computations on the lowest-lying masses are presented in Tables IV, VI, VIII, X, XII, XIV, XVI, XVIII, XX, XXII, XXIV and XXVI, respectively. Therein, the considered meson-meson, diquark-antidiquark and K-type configurations are listed in the first column; if possible, the experimental value of the non-interacting di-meson threshold is labeled in parentheses. In the second column, each channel is assigned with an index which indicates a particular combination of spin ($\chi_j^{\sigma_i}$) and color (χ_j^c) wave functions, that are shown explicitly in the third column. The theoretical mass calculated in each channel is shown in the fourth column, and the coupled result for each kind of configuration is presented in the last one. Note also

that the last row of the table indicates the lowest-lying mass obtained in a complete coupled-channel calculation of real-range.

In a further step, the CSM method is applied to the complete coupled-channel calculation. Figures 2 to 13 show the distribution of complex eigen-energies and, therein, the obtained resonance states are indicated inside circles. Several insights about the nature of found resonances are given by calculating their size, magnetic moment and dominant component, results are listed among Tables V, VII, IX, XI, XIII, XV, XVII, XIX, XXI, XXIII, XXV and XXVII. Particularly, four kinds of quark distances, which are $r_{Q\bar{Q}}$, $r_{\bar{Q}\bar{q}}$, $r_{Q\bar{q}}$ and r_{QQ} are computed. Besides, two sets of results on resonance's dominant components are analyzed according to the discussion in Sec. II, *viz.* only diagonal elements are considered in the calculation of set I, and the addition of off-diagonal ones are employed in set II.

Finally, a summary of our most salient results is presented in Table XXVIII.

A. The $\bar{c}\bar{c}d\bar{c}$ tetraquarks

The $I(J^P) = \frac{1}{2}(0^+)$ sector: Two meson-meson configurations, $\eta_c D$ and $J/\psi D^*$, in both singlet- and hidden-color channels, two diquark-antidiquark structures, $(cc)(\bar{c}\bar{d})$ and $(cc)^*(\bar{c}\bar{d})^*$, along with five K-type arrangements are individually computed in Table IV. The lowest mass corresponds to the color-singlet state $\eta_c D$, 4886 MeV, the other di-meson channel $J/\psi D^*$ with the same color structure is located at 5114 MeV. The scattering nature of these two meson-meson structures can be concluded when compared with threshold's mass. Furthermore, bound states are also not obtained when the single channel calculation is performed in each exotic structure. Particularly, masses of states in both hidden-color and diquark-antidiquark channels are around 5.35 GeV whereas the K-type configurations present masses in the interval 5.19 – 5.84 GeV.

Results on partially coupled-channel study of these eight configurations are then listed in the last column of Table IV. Firstly, the lowest mass remains at 4.89 GeV, hence it is a scattering state of $\eta_c D$. Secondly, the coupling among different channels within the same exotic structure produce remarkable mass shifts for hidden-color, diquark-antidiquark and K-type channels. However, coupled-channel effects are still weak to produce bound states; the lowest coupled-masses of hidden-color and diquark-antidiquark channels are both ~ 5.31 GeV and K-type configurations are within an energy region of 5.15 – 5.31 GeV. In a further step, when 22 channels listed in Table IV are all included in a coupled-channel calculation of real-range, the scattering nature of $\eta_c D$ remains.

Three narrow resonances are obtained when a complete coupled-channel calculation is performed using the complex-range method. Therein, the six scattering states

TABLE IV. Lowest-lying $\bar{c}c\bar{d}c$ tetraquark states with $I(J^P) = \frac{1}{2}(0^+)$ calculated within the real range formulation of the constituent quark model. The allowed meson-meson, diquark-antidiquark and K-type configurations are listed in the first column; when possible, the experimental value of the non-interacting meson-meson threshold is labeled in parentheses. Each channel is assigned an index in the 2nd column, it reflects a particular combination of spin ($\chi_J^{\sigma_i}$) and color (χ_j^c) wave functions that are shown explicitly in the 3rd column. The theoretical mass obtained in each channel is shown in the 4th column and the coupled result for each kind of configuration is presented in the 5th column. When a complete coupled-channels calculation is performed, last row of the table indicates the calculated lowest-lying mass (unit: MeV).

Channel	Index	$\chi_J^{\sigma_i}; \chi_j^c$ [$i; j$]	M	Mixed	
$(\eta_c D)^1(4851)$	1	[1; 1]	4886		
$(J/\psi D^*)^1(5104)$	2	[2; 1]	5114	4886	
$(\eta_c D)^8$	3	[1; 2]	5367		
$(J/\psi D^*)^8$	4	[2; 2]	5338	5305	
$(cc)(\bar{c}\bar{d})$	5	[3; 4]	5354		
$(cc)^*(\bar{c}\bar{d})^*$	6	[4; 3]	5369	5324	
K_1	7	[5; 5]	5311		
	8	[5; 6]	5363		
	9	[6; 5]	5353		
	10	[6; 6]	5253	5157	
K_2	11	[7; 7]	5305		
	12	[7; 8]	5321		
	13	[8; 7]	5187		
	14	[8; 8]	5362	5176	
K_3	15	[9; 10]	5361		
	16	[10; 9]	5349	5313	
	K_4	17	[11; 12]	5370	
		18	[12; 12]	5839	
19		[11; 11]	5758		
K_5	20	[12; 11]	5351	5275	
	21	[13; 14]	5372		
	22	[14; 13]	5336	5307	
Complete coupled-channels:			4886		

of $\eta_c D$, $J/\psi D^*$ and their radial excitations are clearly presented in Fig. 2 with an energy interval from 4.8 to 5.9 GeV. Besides, one stable pole, $5592 - i2.5$ MeV, is found in the top panel of Fig. 2. Meanwhile, two more resonances are obtained in the bottom panel, which is an enlarged part of a dense energy region from 5.70 to 5.85 GeV, whose complex eigenenergies are $5714 - i1.8$ MeV and $5828 - i2.6$ MeV.

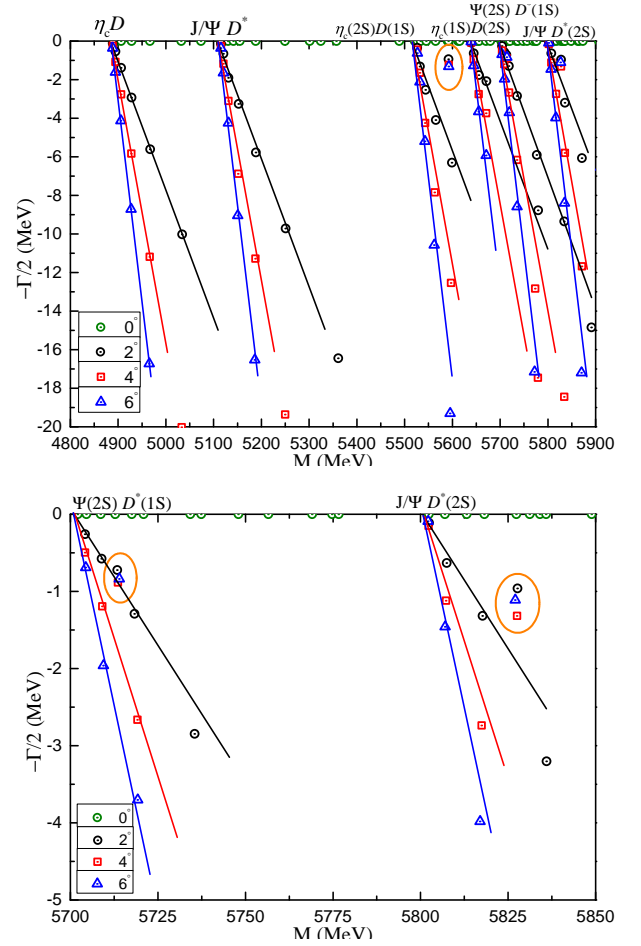


FIG. 2. The complete coupled-channels calculation of $\bar{c}c\bar{d}c$ tetraquark system with $I(J^P) = \frac{1}{2}(0^+)$ quantum numbers. Particularly, the bottom panel is enlarged part of dense energy region from 5.70 GeV to 5.85 GeV.

The resonance electromagnetic and geometric properties, along with their dominant components, are further investigated. Results are summarized in Table V. In particular, the magnetic moment of these three resonances is 0. The lowest resonance at 5.59 GeV is a compact $\bar{c}c\bar{d}c$ tetraquark structure whose size is within 0.96 – 1.42 fm. However, the other two higher resonances present larger sizes, 1.31 – 1.87 fm.

After a comparison of components between Set I and II, one can find that off-diagonal elements contributions are generally small. There is only $\sim 10\%$ modification for diquark-antidiquark and K-type components of the first resonance, and this result also holds for hidden-color and K-type channels of the second one. The third resonance has $\sim 20\%$ modification on the K-type component when off-diagonal elements are included. Accordingly, the dominant components of the three resonances are exotic color configurations of K-type channels. Besides, there are considerable diquark-antidiquark ($\sim 19\%$) and di-meson color-singlet ($\sim 26\%$) components for the resonances at 5.59 GeV and 5.71 GeV, respectively.

TABLE V. Compositeness of exotic resonances obtained in a complete coupled-channel calculation in the $\frac{1}{2}(0^+)$ state of $\bar{c}c\bar{d}c$ tetraquark. Particularly, the first column is resonance poles labeled by $M - i\Gamma$, unit in MeV; the second one is the magnetic moment of resonance, unit in μ_N ; the distance between any two quarks or quark-antiquark, unit in fm; and the component of resonant state (S : dimeson structure in color-singlet channel; H : dimeson structure in hidden-color channel; Di : diquark-antiquark configuration; K : K-type configuration). Herein, two sets of results on a resonance component are listed. Particularly, set I is results on components, that only diagonal elements are employed, and results, that both diagonal and off-diagonal elements are considered, are listed in set II.

Resonance	Structure
5592 - $i2.5$	$\mu = 0$
	$r_{c\bar{c}} : 0.96; r_{\bar{c}d} : 1.42; r_{c\bar{d}} : 1.28; r_{cc} : 1.30$
Set I:	$S : 10.6\%; H : 1.0\%; Di : 29.7\%; K : 58.7\%$
Set II:	$S : 10.0\%; H : 2.1\%; Di : 18.9\%; K : 68.9\%$
5714 - $i1.8$	$\mu = 0$
	$r_{c\bar{c}} : 1.31; r_{\bar{c}d} : 1.87; r_{c\bar{d}} : 1.57; r_{cc} : 1.79$
Set I:	$S : 25.6\%; H : 14.2\%; Di : 6.3\%; K : 53.9\%$
Set II:	$S : 29.6\%; H : 3.5\%; Di : 4.2\%; K : 62.7\%$
5828 - $i2.6$	$\mu = 0$
	$r_{c\bar{c}} : 1.31; r_{\bar{c}d} : 1.82; r_{c\bar{d}} : 1.57; r_{cc} : 1.79$
Set I:	$S : 11.7\%; H : 6.5\%; Di : 15.9\%; K : 65.9\%$
Set II:	$S : 4.3\%; H : 3.5\%; Di : 6.9\%; K : 85.3\%$

The $I(J^P) = \frac{1}{2}(1^+)$ sector: 33 channels should be considered in this case, and our results in real-range calculations are listed in Table VI. Among the three meson-meson configurations, the lowest channel is the color-singlet state of $J/\psi D$, whose theoretical mass, 4994 MeV, is just equal to its non-interacting di-meson theoretical threshold value. Therefore, no bound state is found. This conclusion also holds for the other cases in both single- and coupled-channel computations. Particularly, the remaining two meson-meson channels of $\eta_c D^*$ and $J/\psi D^*$ in color-singlet states locate at 5.01 GeV and 5.11 GeV, respectively. Masses of the three hidden-color channels and three diquark-antidiquark ones converge at 5.35 GeV. 24 K-type channels generally distribute within an energy region of 5.22 - 5.39 GeV. The channels coupling is extremely weak in color-singlet configurations, in contrast to the fact that the mass considerably shifts in coupled-channel calculations of exotic color configurations. As one can see too, all these states are still unstable color resonances in a complete channels coupling calculation.

Figure 3 presents our results on a fully coupled-channel investigation by the CSM. Generally, scattering states of $\eta_c D^*$, $J/\psi D$, $J/\psi D^*$ and their radial excitations are plotted in the top panel, which are located in the en-

TABLE VI. Lowest-lying $\bar{c}c\bar{d}c$ tetraquark states with $I(J^P) = \frac{1}{2}(1^+)$ calculated within the real range formulation of the chiral quark model. Results are similarly organized as those in Table IV (unit: MeV).

Channel	Index	$\chi_{j^i}^{\sigma^i}; \chi_j^c$ [$i; j$]	M	Mixed
$(\eta_c D^*)^1(4988)$	1	[1; 1]	5006	
$(J/\psi D)^1(4967)$	2	[2; 1]	4994	
$(J/\psi D^*)^1(5104)$	3	[3; 1]	5114	4994
$(\eta_c D^*)^8$	4	[1; 2]	5353	
$(J/\psi D)^8$	5	[2; 2]	5358	
$(J/\psi D^*)^8$	6	[3; 2]	5333	5316
$(cc)^*(\bar{c}\bar{d})^*$	7	[6; 3]	5379	
$(cc)^*(\bar{c}\bar{d})$	8	[5; 4]	5342	
$(cc)(\bar{c}\bar{d})^*$	9	[4; 3]	5350	5323
K_1	10	[7; 5]	5359	
	11	[8; 5]	5293	
	12	[9; 5]	5334	
	13	[7; 6]	5336	
	14	[8; 6]	5368	
	15	[9; 6]	5276	5194
K_2	16	[10; 7]	5301	
	17	[11; 7]	5280	
	18	[12; 7]	5219	
	19	[10; 8]	5319	
	20	[11; 8]	5353	
	21	[12; 8]	5345	5201
K_3	22	[13; 10]	5352	
	23	[14; 10]	5372	
	24	[15; 9]	5334	5313
K_4	25	[16; 11]	5385	
	26	[17; 11]	5391	
	27	[18; 11]	5805	
	28	[16; 12]	5382	
	29	[17; 12]	5381	
	30	[18; 12]	5350	5283
K_5	31	[19; 14]	5379	
	32	[20; 14]	5372	
	33	[21; 13]	5322	5306
Complete coupled-channels:				4994

ergy interval 4.95 - 5.90 GeV. Neither bound nor resonant states are obtained below 5.5 GeV. However, a narrow resonance is found at 5693 MeV, and its width is 3.0 MeV. This stable pole can be clearly distin-

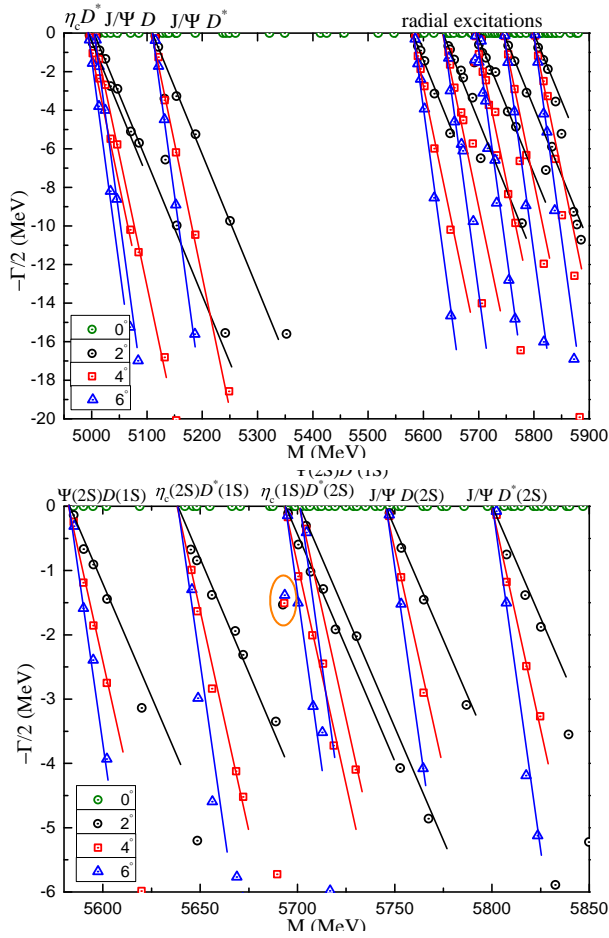


FIG. 3. The complete coupled-channels calculation of $\bar{c}c\bar{d}c$ tetraquark system with $I(J^P) = \frac{1}{2}(1^+)$ quantum numbers. Particularly, the bottom panel is enlarged parts of dense energy region from 5.57 GeV to 5.85 GeV.

TABLE VII. Compositeness of exotic resonance obtained in a complete coupled-channel calculation in the $\frac{1}{2}(1^+)$ state of $\bar{c}c\bar{d}c$ tetraquark. Results are similarly organized as those in Table V.

Resonance	Structure
5693 - $i3.0$	$\mu = -1.06$
	$r_{c\bar{c}} : 1.25; r_{\bar{c}d} : 1.74; r_{c\bar{d}} : 1.34; r_{cc} : 1.61$
Set I:	S: 3.2%; H: 1.1%; Di: 5.5%; K: 90.2%
Set II:	S: 7.7%; H: 4.0%; Di: 9.3%; K: 79.0%

guished in the bottom panel of Fig. 3, where six excited states of $\psi(2S)D(1S)$, $\eta_c(2S)D^*(1S)$, $\eta_c(1S)D^*(2S)$, $\psi(2S)D^*(1S)$, $J/\psi(1S)D(2S)$ and $J/\psi(1S)D^*(2S)$ are shown between 5.57 GeV and 5.85 GeV.

Compositeness of the found resonance is depicted in Table VII. In particular, its magnetic moment is $-1.06\mu_N$, and its size is around 1.25 - 1.74 fm, indicating an extended structure. Our theoretical uncertainty

TABLE VIII. Lowest-lying $\bar{c}c\bar{d}c$ tetraquark states with $I(J^P) = \frac{1}{2}(2^+)$ calculated within the real range formulation of the chiral quark model. Results are similarly organized as those in Table IV (unit: MeV).

Channel	Index	$\chi_{J^i}^{\sigma_i}; \chi_j^c$ [$i; j$]	M	Mixed
$(J/\psi D^*)^1(5104)$	1	[1; 1]	5114	
$(J/\psi D^*)^8$	2	[1; 3]	5358	
$(cc)^*(\bar{c}\bar{d})^*$	3	[1; 7]	5397	
K_1	4	[1; 8]	5348	
	5	[1; 10]	5385	5287
K_2	6	[1; 11]	5335	
	7	[1; 12]	5357	5323
K_3	8	[1; 14]	5393	
K_4	9	[1; 8]	5814	
	10	[1; 10]	5398	5370
K_5	11	[1; 11]	5404	
Complete coupled-channels:				5114

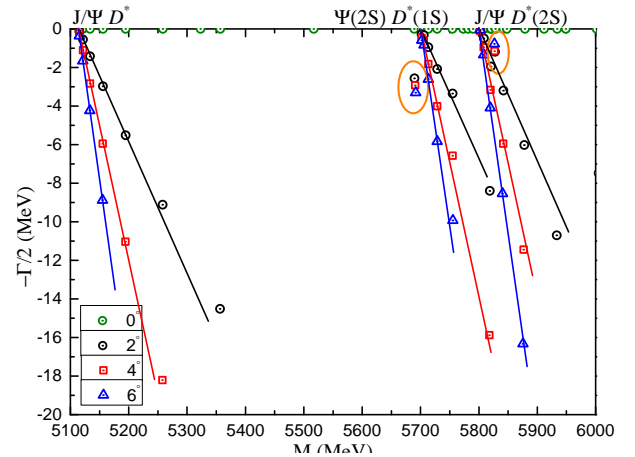


FIG. 4. The complete coupled-channels calculation of $\bar{c}c\bar{d}c$ tetraquark system with $I(J^P) = \frac{1}{2}(2^+)$ quantum numbers.

is less than 12% after comparing the two sets of component results. Hence, the dominant components seems to be exotic, more than 79% comes from K-type configurations.

The $I(J^P) = \frac{1}{2}(2^+)$ state: Table VIII lists 11 channels under investigation for the highest spin state of S-wave $\bar{c}c\bar{d}c$ tetraquark. Firstly, bound states are not present in each kind of real-range calculation, which includes single channel but also partially and complete coupled-channels. Mass of $J/\psi D^*$ in color singlet con-

TABLE IX. Compositeness of exotic resonances obtained in a complete coupled-channel calculation in the $\frac{1}{2}(2^+)$ state of $\bar{c}c\bar{d}c$ tetraquark. Results are similarly organized as those in Table V.

Resonance	Structure
5691 - $i5.9$	$\mu = -1.64$
	$r_{c\bar{c}} : 0.90; r_{\bar{c}\bar{d}} : 1.17; r_{c\bar{d}} : 1.09; r_{cc} : 0.97$
Set I:	$S : 10.4\%; H : 9.2\%; Di : 18.6\%; K : 61.8\%$
Set II:	$S : 17.2\%; H : 3.8\%; Di : 20.7\%; K : 58.3\%$
5827 - $i2.3$	$\mu = -1.64$
	$r_{c\bar{c}} : 1.29; r_{\bar{c}\bar{d}} : 1.77; r_{c\bar{d}} : 1.55; r_{cc} : 1.77$
Set I:	$S : 8.3\%; H : 11.1\%; Di : 19.0\%; K : 61.6\%$
Set II:	$S : 5.3\%; H : 10.3\%; Di : 14.8\%; K : 69.6\%$

figuration is 5114 MeV, and its hidden color case is located at 5358 MeV. Meanwhile, the other exotic color structures are located at ~ 5.40 GeV, except for one K_4 channel with mass of 5.81 GeV.

With a rotated angle varied from 0° to 6° , Fig. 4 shows the distribution of the calculated complex energies. Particularly, in the 5.1 - 6.0 GeV energy region, three scattering states, which are $J/\psi D^*$, $\psi(2S)D^*(1S)$ and $J/\psi D^*(2S)$, are well plotted. Apart from those unstable dots, two resonant poles are circled, their complex energies are 5691 - $i5.9$ and 5827 - $i2.3$, respectively.

The nature of these two resonances can be guessed from Table IX. First of all, their magnetic moments are both $-1.64\mu_N$. However, the geometric structure of these states are different. The lowest resonance is a compact $\bar{c}c\bar{d}c$ tetraquark with a size around 1.1 fm. The higher resonance at 5.8 GeV is a loose structure within 1.29 - 1.77 fm. Modifications in the composition due to off-diagonal elements are less than 8% for both cases. Therefore, one may conclude that K-type configurations are dominant, with more than 60%, and the remaining three configurations, meson-meson in color-singlet and hidden-color plus diquark-antidiquark arrangement, occupies the rest with the same magnitude of proportion.

B. The $\bar{c}c\bar{s}c$ tetraquarks

The $I(J^P) = 0(0^+)$ sector: 22 channels are studied in Table X. Masses of $\eta_c D_s$ and $J/\psi D_s^*$ in the singlet-color channel are 4978 MeV and 5212 MeV, respectively. The hidden-color and diquark-antidiquark channels are all at around 5.45 GeV. Besides, 16 K-type configurations are located at an energy region of 5.31 - 5.95 GeV. Bound states are not obtained in studies of each single channel, and this fact remains in partially and complete coupled-channel calculations. Particularly, the lowest coupled-mass of 7 exotic configuration is ~ 5.4 GeV, except for the K_1 and K_2 structures, whose mass is about 5.3 GeV.

In a further step, when the CSM is employed in a fully

TABLE X. Lowest-lying $\bar{c}c\bar{s}c$ tetraquark states with $I(J^P) = 0(0^+)$ calculated within the real range formulation of the chiral quark model. Results are similarly organized as those in Table IV (unit: MeV).

Channel	Index	$\chi_{J^i}^{\sigma_i}; \chi_J^c$ [$i; j$]	M	Mixed
$(\eta_c D_s)^1(4949)$	1	[1; 1]	4978	
$(J/\psi D_s^*)^1(5209)$	2	[2; 1]	5212	4978
$(\eta_c D_s)^8$	3	[1; 2]	5462	
$(J/\psi D_s^*)^8$	4	[2; 2]	5437	5404
$(cc)(\bar{c}\bar{s})$	5	[3; 4]	5447	
$(cc)^*(\bar{c}\bar{s})^*$	6	[4; 3]	5471	5423
K_1	7	[5; 5]	5422	
	8	[5; 6]	5472	
	9	[6; 5]	5462	
	10	[6; 6]	5363	5269
K_2	11	[7; 7]	5422	
	12	[7; 8]	5432	
	13	[8; 7]	5311	
	14	[8; 8]	5470	5300
K_3	15	[9; 10]	5468	
	16	[10; 9]	5458	5425
K_4	17	[11; 12]	5472	
	18	[12; 12]	5952	
	19	[11; 11]	5881	
	20	[12; 11]	5445	5396
K_5	21	[13; 14]	5477	
	22	[14; 13]	5446	5419
Complete coupled-channels:				4978

coupled-channel investigation, two narrow resonances are obtained. In Fig. 5, whose energy region is from 4.95 GeV to 6.0 GeV, one can find clear distributions of scattering states for $\eta_c D_s$, $J/\psi D_s^*$ and their radial excitations. Moreover, two resonances are obtained in the radial excitation region. In particular, a stable pole is obtained in the top panel, the complex energy reads 5682 - $i4.6$ MeV. As circled in the bottom panel of Fig. 5, there is also another resonance state at 5855 MeV, whose width is 2.8 MeV.

Magnetic moment, quark distance and component distribution are listed in Table XI. Firstly, the μ is 0 for these two resonances. Secondly, the first resonance is an extended object with a size of 1.6 - 2.1 fm; however, the other resonance is compact with a size less than 1.4 fm. The calculated two sets of components indicate a small contribution from off-diagonal elements, the domi-

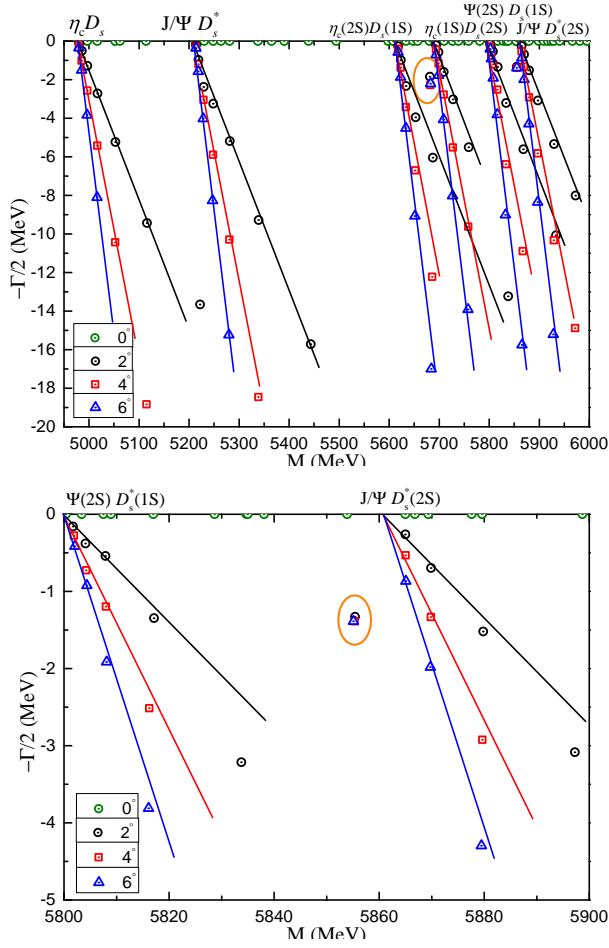


FIG. 5. The complete coupled-channels calculation of $\bar{c}c\bar{s}c$ tetraquark system with $I(J^P) = 0(0^+)$ quantum numbers. Particularly, the bottom panel is enlarged parts of dense energy region from 5.8 GeV to 5.9 GeV.

TABLE XI. Compositeness of the exotic resonances obtained in a complete coupled-channel calculation in the $0(0^+)$ state of $\bar{c}c\bar{s}c$ tetraquark. Results are similarly organized as those in Table V.

Resonance	Structure
5682 - $i4.6$	$\mu = 0$
	$r_{c\bar{c}} : 1.53; r_{\bar{c}\bar{s}} : 2.09; r_{c\bar{s}} : 1.59; r_{cc} : 2.10$
Set I:	$S: 19.7\%; H: 21.8\%; Di: 2.1\%; K: 56.4\%$
Set II:	$S: 29.2\%; H: 12.2\%; Di: 3.5\%; K: 55.1\%$
5855 - $i2.8$	$\mu = 0$
	$r_{c\bar{c}} : 1.07; r_{\bar{c}\bar{s}} : 1.38; r_{c\bar{s}} : 1.12; r_{cc} : 1.36$
Set I:	$S: 17.1\%; H: 22.9\%; Di: 6.3\%; K: 53.7\%$
Set II:	$S: 19.1\%; H: 10.2\%; Di: 10.0\%; K: 60.7\%$

nant ones are color-singlet ($\sim 20\%$) and K-type ($\sim 55\%$) channels for both states.

The $I(J^P) = 0(1^+)$ sector: 33 channels listed in

TABLE XII. Lowest-lying $\bar{c}c\bar{s}c$ tetraquark states with $I(J^P) = 0(1^+)$ calculated within the real range formulation of the chiral quark model. Results are similarly organized as those in Table IV (unit: MeV).

Channel	Index	$\chi_{J^i}^{\sigma^i}; \chi_{J^j}^c$ [$i; j$]	M	Mixed
$(\eta_c D_s^*)^1(5093)$	1	[1; 1]	5104	
$(J/\psi D_s)^1(5065)$	2	[2; 1]	5086	
$(J/\psi D_s^*)^1(5209)$	3	[3; 1]	5212	5086
$(\eta_c D_s^*)^8$	4	[1; 2]	5450	
$(J/\psi D_s)^8$	5	[2; 2]	5453	
$(J/\psi D_s^*)^8$	6	[3; 2]	5433	5415
$(cc)^*(\bar{c}\bar{d})^*$	7	[6; 3]	5480	
$(cc)^*(\bar{c}\bar{d})$	8	[5; 4]	5438	
$(cc)(\bar{c}\bar{d})^*$	9	[4; 3]	5454	5424
K_1	10	[7; 5]	5464	
	11	[8; 5]	5410	
	12	[9; 5]	5445	
	13	[7; 6]	5449	
	14	[8; 6]	5473	
	15	[9; 6]	5383	5303
K_2	16	[10; 7]	5420	
	17	[11; 7]	5400	
	18	[12; 7]	5336	
	19	[10; 8]	5434	
	20	[11; 8]	5459	
	21	[12; 8]	5455	5320
K_3	22	[13; 10]	5462	
	23	[14; 10]	5477	
	24	[15; 9]	5445	5427
K_4	25	[16; 11]	5480	
	26	[17; 11]	5484	
	27	[18; 11]	5921	
	28	[16; 12]	5483	
	29	[17; 12]	5482	
	30	[18; 12]	5454	5401
K_5	31	[19; 14]	5482	
	32	[20; 14]	5479	
	33	[21; 13]	5435	5421
Complete coupled-channels:				5086

Table XII are investigated in this case. Generally, the three meson-meson configurations in singlet-color channels are $\eta_c D_s^*$, $J/\psi D_s$ and $J/\psi D_s^*$. Their lowest-lying masses are 5.10 GeV, 5.09 GeV and 5.21 GeV, respectively. Hence, bound states are still unavailable in this

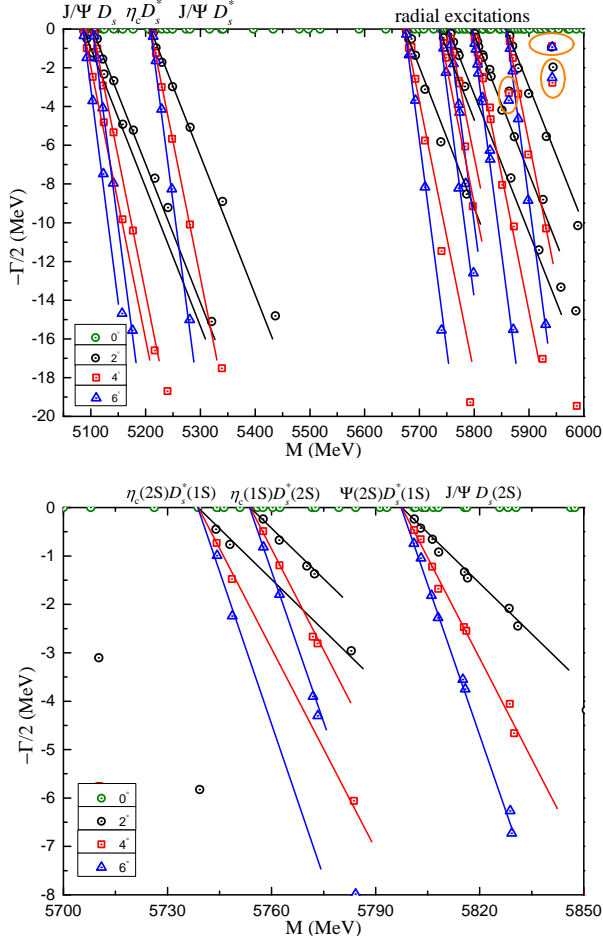


FIG. 6. The complete coupled-channels calculation of $\bar{c}c\bar{s}c$ tetraquark system with $I(J^P) = 0(1^+)$ quantum numbers. Particularly, the bottom panel is enlarged parts of dense energy region from 5.70 GeV to 5.85 GeV.

sector. Masses of the hidden-color, diquark-antidiquark, K_3 and K_5 channels are ~ 5.45 GeV. This value is consistent with most channels in the K_1 , K_2 and K_4 configurations, except for one K_1 channel at 5.38 GeV, one K_2 channel at 5.34 GeV, and one K_4 channel at 5.92 GeV. After partially coupled-channel calculations are performed in each configuration, the lowest-lying mass, which is the non-interacting $J/\psi D_s$ theoretical threshold value, remains at 5.09 GeV. Besides, the extremely weak coupling effect is persistent in a fully coupled-channels study.

In a fully coupled-channel investigation by the CSM, three resonance poles are obtained and they are circled in Fig. 6. Particularly, in the top panel, whose energy ranges within the interval 5.05 – 6.00 GeV, scattering states of the ground and first radial excitations of $\eta_c D_s^*$, $J/\psi D_s$ and $J/\psi D_s^*$ are well presented. Moreover, the energy region from 5.70 GeV to 5.85 GeV is enlarged in the bottom panel. Therein, the four radial excitations, $\eta_c(2S)D_s^*(1S)$, $\eta_c(1S)D_s^*(2S)$, $\psi(2S)D_s^*(1S)$ and $J/\psi D_s(2S)$, are clearly plotted. Apart from the scat-

TABLE XIII. Compositeness of exotic resonances obtained in a complete coupled-channel calculation in the $0(1^+)$ state of $\bar{c}c\bar{s}c$ tetraquark. Results are similarly organized as those in Table V.

Resonance	Structure
5863 – $i6.6$	$\mu = 0.578$
	$r_{c\bar{c}} : 1.62; r_{c\bar{s}} : 2.26; r_{c\bar{s}} : 1.68; r_{cc} : 2.20$
Set I:	$S : 6.6\%; H : 14.6\%; Di : 1.1\%; K : 77.7\%$
Set II:	$S : 3.0\%; H : 21.4\%; Di : 10.2\%; K : 65.4\%$
5941 – $i1.8$	$\mu = 0.503$
	$r_{c\bar{c}} : 1.13; r_{c\bar{s}} : 1.52; r_{c\bar{s}} : 1.33; r_{cc} : 1.53$
Set I:	$S : 21.1\%; H : 7.8\%; Di : 1.3\%; K : 69.8\%$
Set II:	$S : 16.0\%; H : 8.8\%; Di : 5.4\%; K : 69.8\%$
5942 – $i5.6$	$\mu = 0.068$
	$r_{c\bar{c}} : 1.31; r_{c\bar{s}} : 1.95; r_{c\bar{s}} : 1.60; r_{cc} : 1.79$
Set I:	$S : 17.3\%; H : 5.7\%; Di : 0.5\%; K : 76.5\%$
Set II:	$S : 17.8\%; H : 15.6\%; Di : 1.2\%; K : 65.5\%$

tering dots, three stable resonance poles are obtained at around 5.9 GeV. The complex energies are 5863 – $i6.6$ MeV, 5941 – $i1.8$ MeV and 5942 – $i5.6$ MeV.

The nature of three resonances are listed in Table XIII. Considering the magnetic moment, the first two resonances have similar values, $0.578\mu_N$ and $0.503\mu_N$, respectively. However, the value $0.068\mu_N$ is obtained for the third resonance. The size of the resonance at 5.86 GeV is 1.6 – 2.2 fm, and the other two higher resonances present a size less than 1.95 fm. Finally, the K-type channels takes up more than 65% for all of these resonances. Meanwhile, there is also $\sim 20\%$ di-meson configurations in color-singlet channels for resonances at 5.94 GeV. Additionally, the hidden-color channels of the first resonance state have a similar proportion. Herein, the effect of off-diagonal elements is still weak, with less than 13% modification.

The $I(J^P) = 0(2^+)$ sector: There are 11 channels in the highest spin state and Table XIV lists the calculated results. Several conclusions can be drawn. Firstly, no bound state is found in neither a single channel nor a coupled-channel computation. Secondly, the color-singlet channel of $J/\psi D_s^*$ is 5.21 GeV, and the hidden-color channel is 5.45 GeV. Besides, the other exotic color configurations also locate at this energy level, except for one K_4 channel whose mass is 5.93 GeV. One can appreciate a notable mass shift in each K-type configuration when coupling, however, it is not strong enough to produce a bound state.

Figure 7 shows the distribution of complex energies obtained in a complete coupled-channel computation by the CSM. Therein, three scattering states of $J/\psi D_s^*$, $\psi(2S)D_s^*(1S)$ and $J/\psi D_s^*(2S)$ are well presented. Besides, two resonance poles are obtained in the complex plane. Their mass and width are denoted as 5788 – $i3.1$

TABLE XIV. Lowest-lying $\bar{c}c\bar{s}c$ tetraquark states with $I(J^P) = 0(2^+)$ calculated within the real range formulation of the chiral quark model. Results are similarly organized as those in Table IV (unit: MeV).

Channel	Index	$\chi_{J^i}^{\sigma^i}; \chi_j^c$ [$i; j$]	M	Mixed
$(J/\psi D_s^*)^1(5209)$	1	[1; 1]	5212	
$(J/\psi D_s^*)^8$	2	[1; 3]	5452	
$(cc)^*(\bar{c}\bar{d})^*$	3	[1; 7]	5497	
K_1	4	[1; 8]	5459	
	5	[1; 10]	5487	5391
K_2	6	[1; 11]	5448	
	7	[1; 12]	5465	5437
K_3	8	[1; 14]	5496	
K_4	9	[1; 8]	5930	
	10	[1; 10]	5498	5483
K_5	11	[1; 11]	5506	
Complete coupled-channels:			5212	

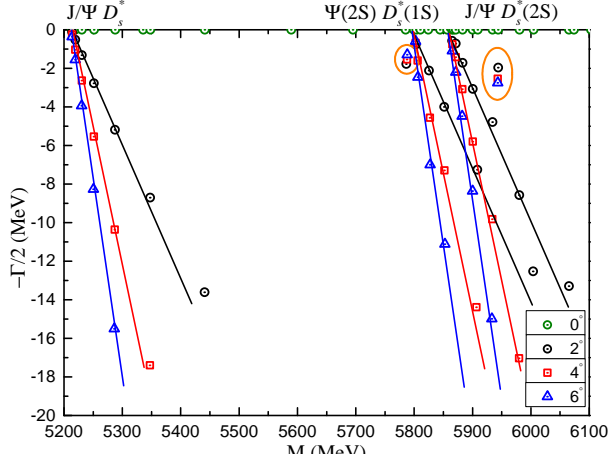


FIG. 7. The complete coupled-channels calculation of $\bar{c}c\bar{s}c$ tetraquark system with $I(J^P) = 0(2^+)$ quantum numbers.

MeV and $5943 - i5.1$ MeV, respectively.

The electromagnetic and geometric properties of the resonances can be found in Table XV. In particular, the magnetic moment of these two resonance states is $0.92\mu_N$. A compact $\bar{c}c\bar{s}c$ tetraquark is obtained for the lower resonance with a size less than 1.10 fm; however, the resonance at 5.94 GeV is an extended object with a size of $1.42 - 2.03$ fm. The dominant wavefunction components of these two states are different, being the dominant ones for the first resonance the hidden-color (35%)

TABLE XV. Compositeness of exotic resonances obtained in a complete coupled-channel calculation in the $0(2^+)$ state of $\bar{c}c\bar{s}c$ tetraquark. Results are similarly organized as those in Table V.

Resonance	Structure
$5788 - i3.1$	$\mu = 0.921$ $r_{c\bar{c}} : 0.84; r_{\bar{c}s} : 1.08; r_{c\bar{s}} : 1.02; r_{cc} : 1.05$ Set I: $S : 7.2\%; H : 35.2\%; Di : 2.6\%; K : 55.0\%$ Set II: $S : 8.5\%; H : 35.5\%; Di : 3.2\%; K : 52.8\%$
$5943 - i5.1$	$\mu = 0.921$ $r_{c\bar{c}} : 1.42; r_{\bar{c}s} : 2.03; r_{c\bar{s}} : 1.65; r_{cc} : 1.96$ Set I: $S : 9.0\%; H : 2.5\%; Di : 2.0\%; K : 86.5\%$ Set II: $S : 18.4\%; H : 6.4\%; Di : 8.7\%; K : 66.5\%$

and K-type (55%) channels while, for the second resonance, one has the color-singlet (18%) and K-type (67%) configurations as the dominant ones. There is almost no difference between sets I and II for the component assessment of the first resonance, and the difference is small for the second one.

C. The $\bar{b}b\bar{d}b$ tetraquarks

The $I(J^P) = \frac{1}{2}(0^+)$ sector: 22 channels are studied in this quantum state; particularly, there are two channels in the color-singlet, hidden-color and diquark-antidiquark configurations, respectively. The other 16 channels are from the K-type structures. As shown in Table XVI, within real-range method, the lowest-lying channel is an $\eta_b B$ scattering state with mass at 14.73 GeV, and the mass of ΥB^* state is 14.82 GeV. The other channels are at ~ 15.05 GeV, except for two K_4 channels with masses 15.36 GeV and 15.46 GeV, respectively. The effect of channel coupling is weak. The lowest-lying mass remains at 14.73 GeV, K_1 and K_2 configurations are almost degenerate in mass, 14.89 GeV, and the other coupled-mass of exotic structures are at around 15.0 GeV.

The computed complex energies obtained from a fully-coupled channels CSM calculation are plotted in Fig. 8. Firstly, $\eta_b B$ and ΥB^* in both ground and radial excited states are clearly shown in the top panel (energy region 14.7 – 15.6 GeV). Meanwhile, four radial excitations, $\eta_b(2S)B(1S)$, $\Upsilon(2S)B^*(1S)$, $\eta_b(1S)B(2S)$ and $\Upsilon(1S)B^*(2S)$ are presented in the bottom panel, which is an enlarged part of the energy region from 15.25 to 15.55 GeV. Apart from these scattering states, four resonance states are observed with complex energies $15320 - i0.5$ MeV, $15331 - i4.5$ MeV, $15372 - i6.1$ MeV and $15407 - i9.3$ MeV. In particular, the two resonances at 15.33 GeV and 15.41 GeV are consistent with those obtained in Ref. [30].

The nature of these resonances can be guessed from Table XVII. Firstly, their magnetic moment are all 0.

TABLE XVI. Lowest-lying $\bar{b}b\bar{d}b$ tetraquark states with $I(J^P) = \frac{1}{2}(0^+)$ calculated within the real range formulation of the chiral quark model. Results are similarly organized as those in Table IV (unit: MeV).

Channel	Index	$\chi_{J^i}^{\sigma_i}; \chi_j^c$ [$i; j$]	M	Mixed
$(\eta_b B)^1(14580)$	1	[1; 1]	14732	
$(\Upsilon B^*)^1(14785)$	2	[2; 1]	14824	14732
$(\eta_b B)^8$	3	[1; 2]	15050	
$(\Upsilon B^*)^8$	4	[2; 2]	15049	15020
$(bb)(\bar{b}\bar{d})$	5	[3; 4]	15042	
$(bb)^*(\bar{b}\bar{d})^*$	6	[4; 3]	15061	15034
K_1	7	[5; 5]	15021	
	8	[5; 6]	15001	
	9	[6; 5]	15028	
	10	[6; 6]	14964	14898
K_2	11	[7; 7]	14952	
	12	[7; 8]	15027	
	13	[8; 7]	14908	
	14	[8; 8]	15035	14894
K_3	15	[9; 10]	15053	
	16	[10; 9]	15025	15017
K_4	17	[11; 12]	15063	
	18	[12; 12]	15457	
	19	[11; 11]	15364	
	20	[12; 11]	15036	14959
K_5	21	[13; 14]	15063	
	22	[14; 13]	15016	15010
Complete coupled-channels:				14732

Secondly, they are relatively extended structures, with sizes of 1.0 – 1.7 fm. Thirdly, their dominant wavefunction components are K-type channels but there are also considerable diquark-antidiquark components. Note that the differences between set I and II is less than 17% after comparison.

The $I(J^P) = \frac{1}{2}(1^+)$ sector: 33 channels have to be studied for this quantum state and they are shown in Table XVIII. The three meson-meson configurations of $\eta_b B^*$, ΥB and ΥB^* in color-singlet channels are all unbound. Their lowest-lying masses just equal to the corresponding theoretical threshold values, *i.e.* 14.77 GeV, 14.78 GeV and 14.82 GeV, respectively. The hidden-color channels are almost degenerate in mass at around 15.04 GeV. Meanwhile, the three diquark-antidiquark channels locate at ~ 15.05 GeV. Masses of the 24 K-type channels are generally within an energy region from 14.92 GeV to

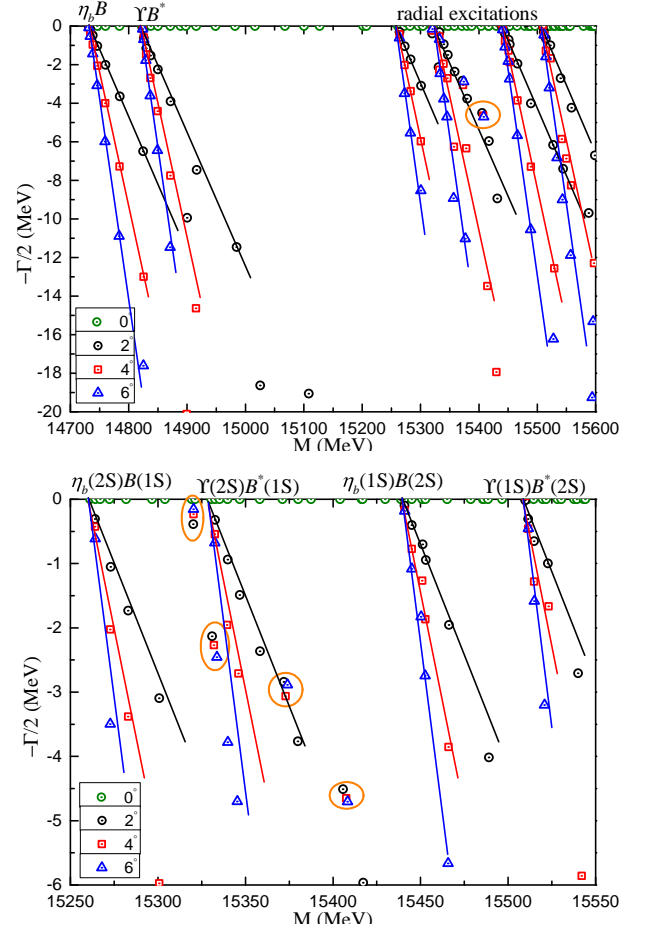


FIG. 8. The complete coupled-channels calculation of $\bar{b}b\bar{d}b$ tetraquark system with $I(J^P) = \frac{1}{2}(0^+)$ quantum numbers. Particularly, the bottom panel is enlarged parts of dense energy region from 15.25 GeV to 15.55 GeV.

15.39 GeV. Coupled-channels effect helps a little in pushing the lowest mass down and it is still weak to obtain a bound state in each kind of calculation.

In a further step towards a complex-range study of complete coupled-channels calculation, four resonance states are obtained and they are circled in Fig. 9. Particularly, three panels are presented. The energy point distributions of $1S$ and $2S$ states of the system are plotted in the top panel with an energy region 14.75 – 15.60 GeV. Since there are dense distributions of energy dots in 14.77 – 14.97 GeV and 15.28 – 15.58 GeV, enlarged parts of these two energy regions are plotted in the middle and bottom panels, respectively. Firstly, three scattering states of $\eta_b B^*$, ΥB and ΥB^* are well presented in the middle panel of Fig. 9. Besides, six radial excitation states, which include $\Upsilon(2S)B(1S)$, $\eta_b(2S)B^*(1S)$, $\Upsilon(2S)B^*(1S)$, $\eta_b(1S)B^*(2S)$, $\Upsilon(1S)B(2S)$ and $\Upsilon(1S)B^*(2S)$, are also shown in the bottom one. Therein, four stable poles are obtained, the resonance states are $15327 - i1.5$ MeV, $15376 - i3.2$ MeV, $15395 - i4.2$ MeV and $15417 - i10.2$

TABLE XVII. Compositeness of exotic resonances obtained in a complete coupled-channel calculation in the $\frac{1}{2}(0^+)$ state of $\bar{b}b\bar{d}b$ tetraquark. Results are similarly organized as those in Table V.

Resonance	Structure
15320 - $i0.5$	$\mu = 0$ $r_{b\bar{b}} : 0.96; r_{\bar{b}d} : 1.52; r_{b\bar{d}} : 1.26; r_{bb} : 1.33$ <i>Set I:</i> $S : 6.0\%; H : 0.6\%; Di : 21.2\%; K : 72.2\%$ <i>Set II:</i> $S : 8.2\%; H : 0.1\%; Di : 4.1\%; K : 87.6\%$
15331 - $i4.5$	$\mu = 0$ $r_{b\bar{b}} : 1.23; r_{\bar{b}d} : 1.77; r_{b\bar{d}} : 1.32; r_{bb} : 1.64$ <i>Set I:</i> $S : 2.5\%; H : 1.6\%; Di : 25.1\%; K : 70.8\%$ <i>Set II:</i> $S : 4.5\%; H : 2.5\%; Di : 23.2\%; K : 69.8\%$
15372 - $i6.1$	$\mu = 0$ $r_{b\bar{b}} : 1.12; r_{\bar{b}d} : 1.70; r_{b\bar{d}} : 1.37; r_{bb} : 1.54$ <i>Set I:</i> $S : 2.5\%; H : 0.7\%; Di : 20.9\%; K : 75.9\%$ <i>Set II:</i> $S : 6.2\%; H : 5.8\%; Di : 16.6\%; K : 71.4\%$
15407 - $i9.3$	$\mu = 0$ $r_{b\bar{b}} : 1.05; r_{\bar{b}d} : 1.59; r_{b\bar{d}} : 1.31; r_{bb} : 1.45$ <i>Set I:</i> $S : 1.2\%; H : 1.0\%; Di : 23.7\%; K : 74.1\%$ <i>Set II:</i> $S : 4.5\%; H : 3.1\%; Di : 22.7\%; K : 69.7\%$

MeV, respectively. Moreover, the later three resonances are also compatible with results in Ref. [30].

Table XIX summarizes properties of the four resonance states. First of all, magnetic moments of them are negative: $-1.453\mu_N$, $-1.817\mu_N$, $-1.456\mu_N$ and $-1.771\mu_N$, respectively. Their sizes are within the range 1.0–1.6 fm. The dominant components ($> 70\%$) are K-type channels, and there are also considerable diquark-antidiquark components. The influence of off-diagonal elements continues to be small in this sector.

The $I(J^P) = \frac{1}{2}(2^+)$ sector: The ΥB^* in both color-singlet and hidden-color channels, a $(bb)^*(\bar{b}\bar{d})^*$ channel, along with 8 K-type channels are comprehensively studied in Table XX. A bound state is still excluded in this sector, and the lowest-lying mass is 14.82 GeV, which is the ΥB^* theoretical threshold value. The other channels locate within 14.99 – 15.39 GeV energy interval. In coupled-channel calculations, the lowest-lying mass of each K-type configuration is ~ 15.0 GeV.

Three resonances are obtained in a complete coupled-channel by the CSM. Figure 10 shows the distribution of complex energies within 14.8 – 15.6 GeV. Apart from three scattering states of ΥB^* , $\Upsilon(2S)B^*(1S)$ and $\Upsilon(1S)B^*(2S)$, three stable poles are circled. The resonances are 15308 - $i9.3$ MeV, 15449 - $i1.4$ MeV and 15558 - $i5.4$ MeV.

In Table XXI one can find that the magnetic moment of the three resonance states is approximately $-2.1\mu_N$. Besides, a compact $\bar{b}b\bar{d}b$ tetraquark structure is found

TABLE XVIII. Lowest-lying $\bar{b}b\bar{d}b$ tetraquark states with $I(J^P) = \frac{1}{2}(1^+)$ calculated within the real range formulation of the chiral quark model. Results are similarly organized as those in Table IV (unit: MeV).

Channel	Index	$\chi_J^{\sigma i}; \chi_j^c$ [$i; j$]	M	Mixed
$(\eta_b B^*)^1(14625)$	1	[1; 1]	14773	
$(\Upsilon B)^1(14740)$	2	[2; 1]	14783	
$(\Upsilon B^*)^1(14785)$	3	[3; 1]	14824	14773
$(\eta_b B^*)^8$	4	[1; 2]	15043	
$(\Upsilon B)^8$	5	[2; 2]	15046	
$(\Upsilon B^*)^8$	6	[3; 2]	15041	15022
$(bb)^*(\bar{b}\bar{d})^*$	7	[6; 3]	15065	
$(bb)^*(\bar{b}\bar{d})$	8	[5; 4]	15036	
$(bb)(\bar{b}\bar{d})^*$	9	[4; 3]	15053	15031
K_1	10	[7; 5]	15040	
	11	[8; 5]	14998	
	12	[9; 5]	15020	
	13	[7; 6]	14991	
	14	[8; 6]	15027	
	15	[9; 6]	14976	14913
K_2	16	[10; 7]	14972	
	17	[11; 7]	14940	
	18	[12; 7]	14923	
	19	[10; 8]	15010	
	20	[11; 8]	15042	
	21	[12; 8]	15027	14904
K_3	22	[13; 10]	15048	
	23	[14; 10]	15058	
	24	[15; 9]	15018	15014
K_4	25	[16; 11]	15067	
	26	[17; 11]	15081	
	27	[18; 11]	15387	
	28	[16; 12]	15070	
	29	[17; 12]	15069	
	30	[18; 12]	15055	14963
K_5	31	[19; 14]	15066	
	32	[20; 14]	15062	
	33	[21; 13]	15009	15006
Complete coupled-channels:				14773

for the first resonance whereas the size of the other two states is larger. Furthermore, diquark-antidiquark and K-type channels are the dominant components ($> 90\%$) of these three resonances.

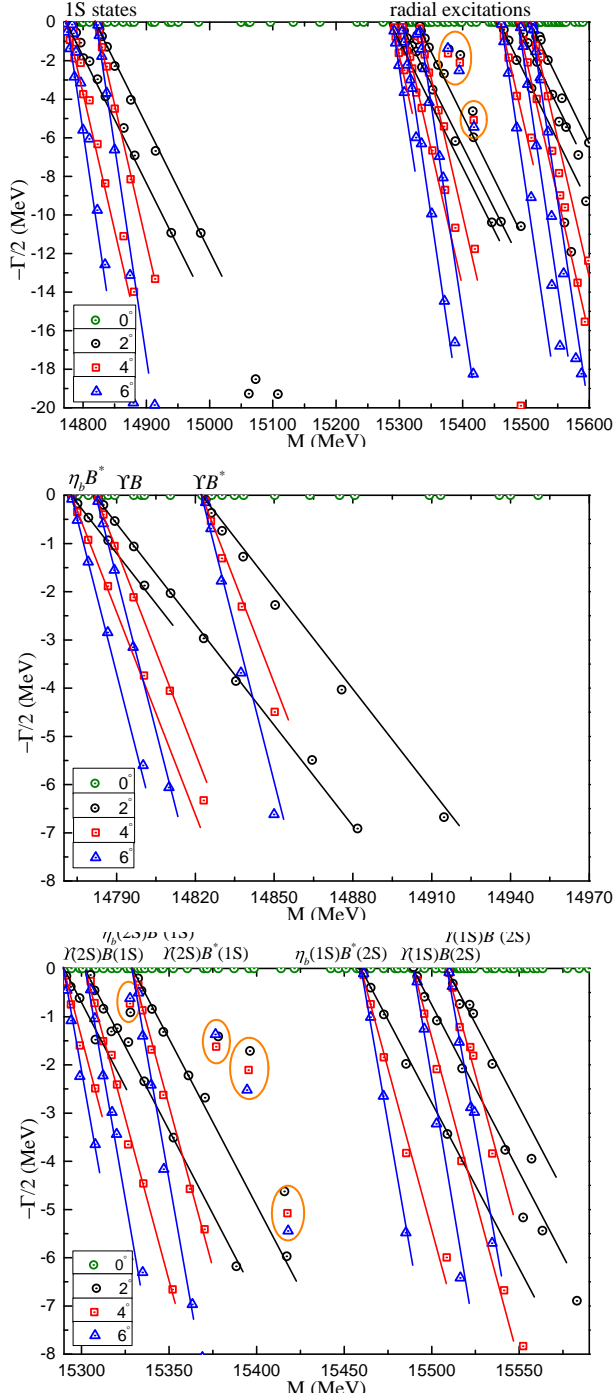


FIG. 9. The complete coupled-channels calculation of $\bar{b}b\bar{u}b$ tetraquark system with $I(J^P) = \frac{1}{2}(1^+)$ quantum numbers. Particularly, the middle panel is enlarged parts of dense energy region from 14.77 GeV to 14.97 GeV, and the bottom one is enlarged parts of dense energy region from 15.28 GeV to 15.58 GeV.

D. The $\bar{b}b\bar{s}b$ tetraquarks

The $I(J^P) = 0(0^+)$ sector: Firstly, two meson-meson configurations, $\eta_b B_s$ and ΥB_s^* , are studied in both

TABLE XIX. Compositeness of exotic resonances obtained in a complete coupled-channel calculation in the $\frac{1}{2}(1^+)$ state of $\bar{b}b\bar{d}b$ tetraquark. Results are similarly organized as those in Table V.

Resonance	Structure
15327 - i1.5	$\mu = -1.453$ $r_{b\bar{b}} : 1.08; r_{\bar{b}\bar{d}} : 1.58; r_{b\bar{d}} : 1.22; r_{bb} : 1.44$
Set I:	$S : 1.9\%; H : 1.5\%; Di : 26.3\%; K : 70.3\%$
Set II:	$S : 1.4\%; H : 4.0\%; Di : 8.4\%; K : 86.2\%$
15376 - i3.2	$\mu = -1.817$ $r_{b\bar{b}} : 1.04; r_{\bar{b}\bar{d}} : 1.63; r_{b\bar{d}} : 1.33; r_{bb} : 1.43$
Set I:	$S : 1.1\%; H : 1.1\%; Di : 24.9\%; K : 72.9\%$
Set II:	$S : 3.9\%; H : 6.2\%; Di : 13.4\%; K : 76.5\%$
15395 - i4.2	$\mu = -1.456$ $r_{b\bar{b}} : 0.95; r_{\bar{b}\bar{d}} : 1.48; r_{b\bar{d}} : 1.26; r_{bb} : 1.31$
Set I:	$S : 1.6\%; H : 0.7\%; Di : 14.8\%; K : 82.9\%$
Set II:	$S : 5.4\%; H : 3.1\%; Di : 12.3\%; K : 79.2\%$
15417 - i10.2	$\mu = -1.771$ $r_{b\bar{b}} : 0.99; r_{\bar{b}\bar{d}} : 1.48; r_{b\bar{d}} : 1.20; r_{bb} : 1.36$
Set I:	$S : 2.7\%; H : 0.5\%; Di : 17.5\%; K : 79.3\%$
Set II:	$S : 5.4\%; H : 1.5\%; Di : 2.9\%; K : 90.2\%$

TABLE XX. Lowest-lying $\bar{b}b\bar{d}b$ tetraquark states with $I(J^P) = \frac{1}{2}(2^+)$ calculated within the real range formulation of the chiral quark model. Results are similarly organized as those in Table IV (unit: MeV).

Channel	Index	$\chi_{J^i}^{\sigma_i}; \chi_j^c$ [$i; j$]	M	Mixed
$(\Upsilon B^*)^1(14785)$	1	[1; 1]	14824	
$(\Upsilon B^*)^8$	2	[1; 3]	15040	
$(bb)^*(\bar{b}\bar{d})^*$	3	[1; 7]	15073	
K_1	4	[1; 8]	15020	
	5	[1; 10]	15038	14964
K_2	6	[1; 11]	14986	
	7	[1; 12]	15027	14977
K_3	8	[1; 14]	15067	
K_4	9	[1; 8]	15391	
	10	[1; 10]	15075	15021
K_5	11	[1; 11]	15077	
Complete coupled-channels:			14824	

color-singlet and hidden-color channels. No bound state

TABLE XXI. Compositeness of exotic resonances obtained in a complete coupled-channel calculation in the $\frac{1}{2}(2^+)$ state of $\bar{b}\bar{b}\bar{d}\bar{b}$ tetraquark. Results are similarly organized as those in Table V.

Resonance	Structure
15308 - i 9.3	$\mu = -2.061$ $r_{b\bar{b}} : 0.64; r_{\bar{b}\bar{d}} : 0.92; r_{b\bar{d}} : 0.81; r_{bb} : 0.62$
Set I:	$S : 4.8\%; H : 4.0\%; Di : 19.0\%; K : 72.2\%$
Set II:	$S : 0.6\%; H : 8.8\%; Di : 25.6\%; K : 65.0\%$
15449 - i 1.4	$\mu = -2.061$ $r_{b\bar{b}} : 0.79; r_{\bar{b}\bar{d}} : 1.29; r_{b\bar{d}} : 1.19; r_{bb} : 1.07$
Set I:	$S : 3.7\%; H : 2.4\%; Di : 24.2\%; K : 69.7\%$
Set II:	$S : 3.2\%; H : 5.1\%; Di : 12.8\%; K : 78.9\%$
15558 - i 5.4	$\mu = -2.061$ $r_{b\bar{b}} : 1.00; r_{\bar{b}\bar{d}} : 1.54; r_{b\bar{d}} : 1.30; r_{bb} : 1.22$
Set I:	$S : 2.2\%; H : 3.4\%; Di : 31.6\%; K : 62.8\%$
Set II:	$S : 1.2\%; H : 2.8\%; Di : 26.7\%; K : 69.3\%$

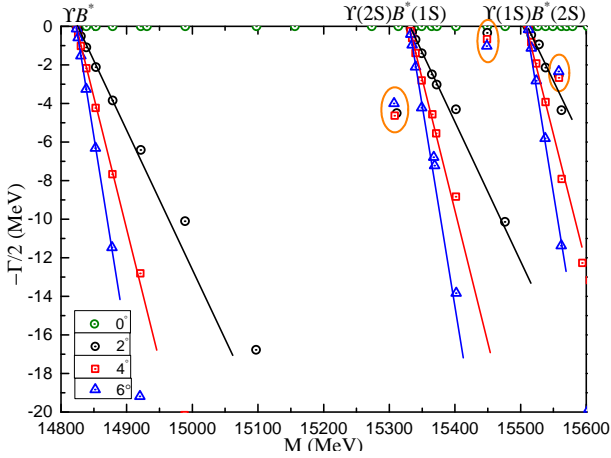


FIG. 10. The complete coupled-channels calculation of $\bar{b}\bar{b}\bar{u}\bar{b}$ tetraquark system with $I(J^P) = \frac{1}{2}(2^+)$ quantum numbers.

is found, the theoretical thresholds of these two cases are 14.81 GeV and 14.91 GeV, respectively. Besides, the two hidden-color channels are almost degenerate at 15.14 GeV. As for the rest channels, diquark-antidiquark and K-type, their masses are ~ 15.10 GeV, except for two K_4 channels which are 15.48 GeV and 15.56 GeV, respectively. We do not find bound states in partially and fully coupled-channel real-range calculations, the lowest-lying mass remains at 14.81 GeV. Meanwhile, the coupled-mass is 14.99 GeV for both K_1 and K_2 states, and the other exotic structures are around 15.1 GeV.

Four resonance states are available in a CSM fully coupled-channel investigation. Scattering energy dots of $\eta_b B_s^*$ and ΥB_s^* in both ground and radial excitations are well presented in Fig. 11. One narrow resonance is also

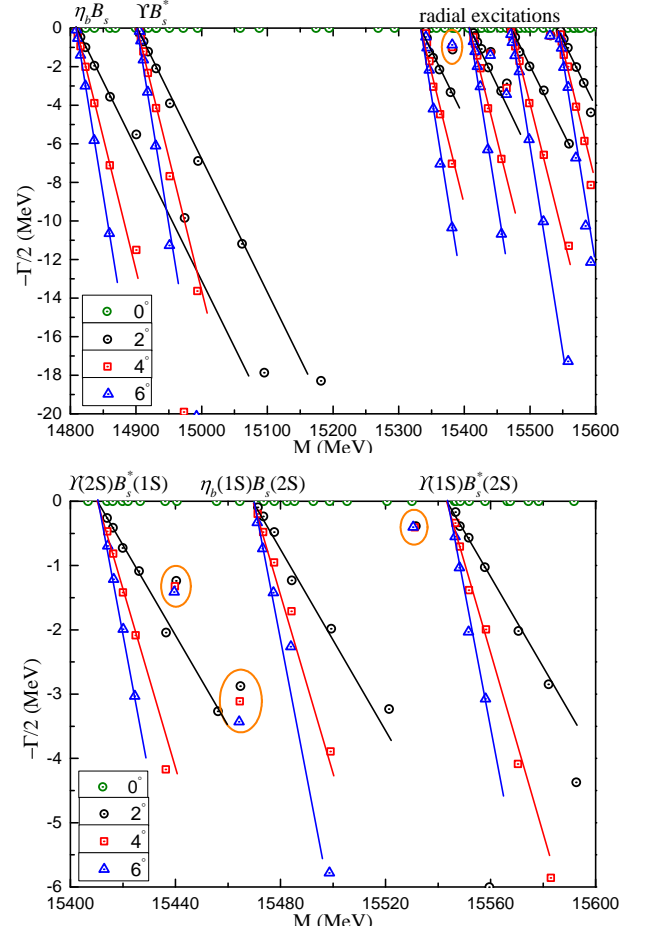


FIG. 11. The complete coupled-channels calculation of $\bar{b}\bar{b}\bar{s}\bar{b}$ tetraquark system with $I(J^P) = 0(0^+)$ quantum numbers. Particularly, the bottom panel is enlarged parts of dense energy region from 15.4 GeV to 15.6 GeV.

found in the top panel of Fig. 11, and three more resonances are circled in the bottom panel. Complex energies of these resonances are 15381 - i 2.0 MeV, 15439 - i 2.6 MeV, 15464 - i 6.2 MeV and 15531 - i 0.8 MeV, respectively. Furthermore, the second resonance at 15.44 GeV is quite compatible with the result in Ref. [30].

Table XXIII list electromagnetic, geometric and wavefunction component properties of the found resonances. The magnetic moment μ is 0 for all of the four resonances. Compact structure is concluded for resonances at 15.38 GeV and 15.53 GeV, whereas the other two seems to be more extended objects. The dominant wavefunction components are of K-type for all these four and they are larger than 70% of the total.

The $I(J^P) = 0(1^+)$ sector: Table XXIV lists the 33 channels under investigation for this quantum state. Firstly, masses of the color-singlet channels $\eta_b B_s^*$, ΥB_s^* and ΥB_s^* are 14.85 GeV, 14.86 GeV and 14.91 GeV, respectively. The three hidden-color channels are almost degenerate with mass ~ 15.13 GeV. Furthermore, diquark-antidiquark and K-type channels are also locate

TABLE XXII. Lowest-lying $\bar{b}b\bar{s}b$ tetraquark states with $I(J^P) = 0(0^+)$ calculated within the real range formulation of the chiral quark model. Results are similarly organized as those in Table IV (unit: MeV).

Channel	Index	$\chi_{J^i}^{\sigma}; \chi_j^c$ [$i; j$]	M	Mixed
$(\eta_b B_s)^1(14667)$	1	[1; 1]	14809	
$(\Upsilon B_s^*)^1(14875)$	2	[2; 1]	14905	14809
$(\eta_b B_s)^8$	3	[1; 2]	15138	
$(\Upsilon B_s^*)^8$	4	[2; 2]	15137	15109
$(bb)(\bar{b}\bar{s})$	5	[3; 4]	15129	
$(bb)^*(\bar{b}\bar{s})^*$	6	[4; 3]	15149	15122
K_1	7	[5; 5]	15111	
	8	[5; 6]	15103	
	9	[6; 5]	15119	
	10	[6; 6]	15067	14993
K_2	11	[7; 7]	15052	
	12	[7; 8]	15118	
	13	[8; 7]	15011	
	14	[8; 8]	15127	14997
K_3	15	[9; 10]	15142	
	16	[10; 9]	15117	15109
K_4	17	[11; 12]	15150	
	18	[12; 12]	15555	
	19	[11; 11]	15477	
	20	[12; 11]	15124	15065
K_5	21	[13; 14]	15152	
	22	[14; 13]	15107	15101
Complete coupled-channels:				14809

at around 15.1 GeV, except for a K_4 channel with a mass of 15.50 GeV. Bound states are not found and coupled-channel calculations do not change this fact. In particular, the lowest mass remains at 14.85 GeV in the color-singlet and fully coupled-channel computations, the other configurations masses are in an energy region of 15.0 – 15.1 GeV.

Four resonances are obtained in a complex-range assessment of the fully-coupled channels case. Figure 12 shows the distribution of complex energy dots within the range 14.85 – 15.70 GeV. The ground and radial excitations show scattering nature and they are presented in the top panel. An enlarged part of 14.85 – 14.95 GeV energy region is shown in the middle panel. Therein, the $\eta_b B_s^*$, ΥB_s and ΥB_s^* scattering states are well identified. In the bottom panel of Fig. 12, whose energy interval is 15.35 – 15.60

TABLE XXIII. Compositeness of exotic resonances obtained in a complete coupled-channel calculation in the $0(0^+)$ state of $\bar{b}b\bar{s}b$ tetraquark. Results are similarly organized as those in Table V.

Resonance	Structure
15381 – $i2.0$	$\mu = 0$ $r_{b\bar{b}} : 0.69; r_{\bar{b}s} : 1.10; r_{b\bar{s}} : 1.01; r_{bb} : 0.92$
Set I:	$S : 17.2\%; H : 5.3\%; Di : 8.2\%; K : 69.3\%$
Set II:	$S : 11.2\%; H : 6.4\%; Di : 9.0\%; K : 73.4\%$
15439 – $i2.6$	$\mu = 0$ $r_{b\bar{b}} : 1.52; r_{\bar{b}s} : 2.17; r_{b\bar{s}} : 1.62; r_{bb} : 2.11$
Set I:	$S : 1.6\%; H : 0.8\%; Di : 1.9\%; K : 95.7\%$
Set II:	$S : 6.9\%; H : 4.4\%; Di : 1.2\%; K : 87.5\%$
15464 – $i6.2$	$\mu = 0$ $r_{b\bar{b}} : 1.31; r_{\bar{b}s} : 1.89; r_{b\bar{s}} : 1.43; r_{bb} : 1.81$
Set I:	$S : 2.5\%; H : 1.9\%; Di : 2.7\%; K : 92.9\%$
Set II:	$S : 6.8\%; H : 6.1\%; Di : 5.6\%; K : 81.5\%$
15531 – $i0.8$	$\mu = 0$ $r_{b\bar{b}} : 0.88; r_{\bar{b}s} : 1.31; r_{b\bar{s}} : 1.14; r_{bb} : 1.22$
Set I:	$S : 1.4\%; H : 1.2\%; Di : 3.1\%; K : 94.3\%$
Set II:	$S : 1.2\%; H : 3.5\%; Di : 7.8\%; K : 87.5\%$

GeV, six $2S$ states of $\bar{b}b\bar{s}b$ tetraquarks are well presented: $\Upsilon(2S)B_s(1S)$, $\eta_b(2S)B_s^*(1S)$, $\Upsilon(2S)B_s^*(1S)$, $\eta_b(1S)B_s^*(2S)$, $\Upsilon(1S)B_s(2S)$ and $\Upsilon(1S)B_s^*(2S)$. Among most unstable dots, four resonance poles are circled, the complex energies read as 15440 – $i2.6$ MeV, 15531 – $i0.4$ MeV, 15632 – $i3.2$ MeV and 15653 – $i6.3$ MeV.

Some insights about the nature of these resonances can be found in Table XXV. Considering the electromagnetic structure the magnetic moment is $0.382\mu_N$, $0.496\mu_N$, $0.355\mu_N$ and $0.226\mu_N$ for each state. Meanwhile, the first two resonances have similar properties related to their size and components. Particularly, their inner quark distances are both within 1.0 – 1.49 fm and K-type channels dominate. There are also common features for the other two resonance states. Their sizes are 0.8 – 1.2 fm and more than 80% is of K-type component.

The $I(J^P) = 0(2^+)$ sector: Table XXVI lists the calculated results on the highest spin state of $\bar{b}b\bar{s}b$ tetraquark. Bound states remain unavailable. The masses of the color-singlet and hidden-color channels of ΥB_s^* are 14.91 GeV and 15.13 GeV, respectively. The $(bb)^*(\bar{b}\bar{s})^*$ channel is slightly higher in mass, at 15.16 GeV. Eight K-type channels are generally located at an energy interval from 15.09 GeV to 15.50 GeV. The lowest-lying mass is around 15.10 GeV when partially coupled-channel calculations are performed in the K_1 , K_2 and K_4 configurations.

When performing a fully-coupled channels investigation within the CSM method, three scattering states of

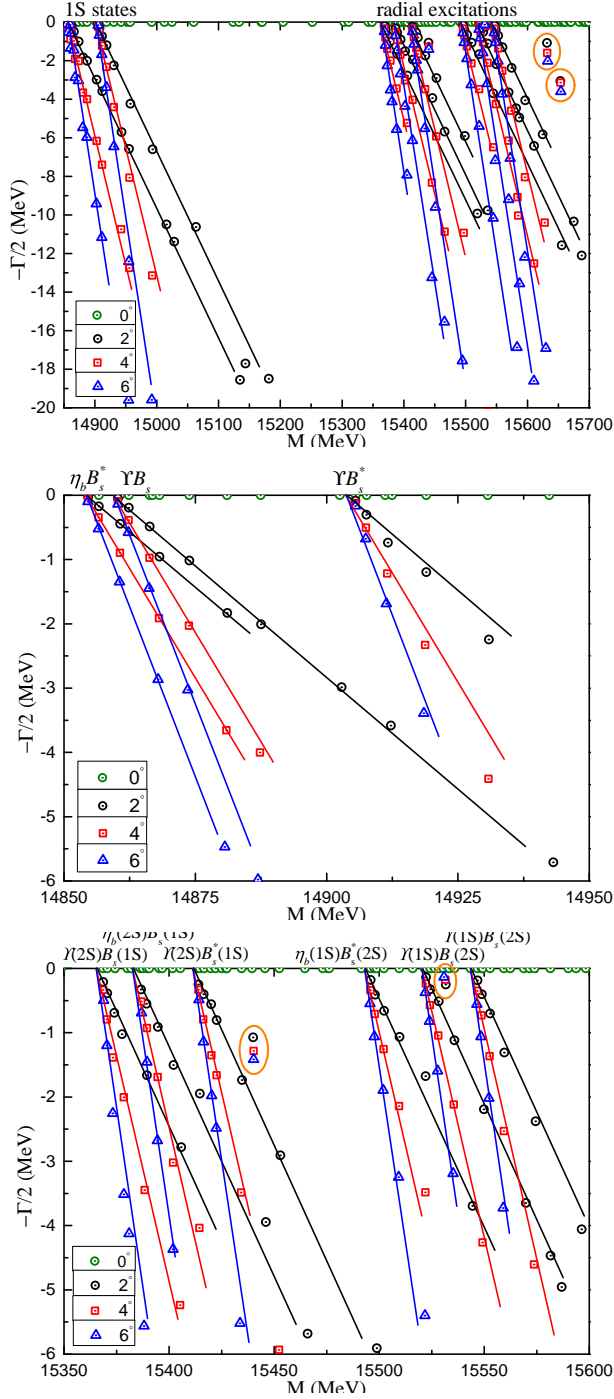


FIG. 12. The complete coupled-channels calculation of $\bar{b}b\bar{s}b$ tetraquark system with $I(J^P) = 0(1^+)$ quantum numbers. Particularly, the middle panel is enlarged parts of dense energy region from 14.85 GeV to 14.95 GeV, and the bottom one is enlarged parts of dense energy region from 15.35 GeV to 15.60 GeV.

ΥB_s^* , $\Upsilon(2S)B_s^*(1S)$ and $\Upsilon(1S)B_s^*(2S)$ are clearly presented in the 14.9 – 15.7 GeV energy region of Fig. 13. Two narrow resonances are obtained in the complex plane, $15405 - i7.6$ MeV and $15669 - i4.2$ MeV. In par-

TABLE XXIV. Lowest-lying $\bar{b}b\bar{s}b$ tetraquark states with $I(J^P) = 0(1^+)$ calculated within the real range formulation of the chiral quark model. Results are similarly organized as those in Table IV (unit: MeV).

Channel	Index	$\chi_J^{\sigma i}; \chi_j^c$ [$i; j$]	M	Mixed
$(\eta_b B_s^*)^1(14715)$	1	[1; 1]	14854	
$(\Upsilon B_s)^1(14827)$	2	[2; 1]	14860	
$(\Upsilon B_s^*)^1(14875)$	3	[3; 1]	14905	14854
$(\eta_b B_s^*)^8$	4	[1; 2]	15132	
$(\Upsilon B_s)^8$	5	[2; 2]	15134	
$(\Upsilon B_s^*)^8$	6	[3; 2]	15130	15111
$(bb)^*(\bar{b}\bar{s})^*$	7	[6; 3]	15153	
$(bb)^*(\bar{b}\bar{s})$	8	[5; 4]	15124	
$(bb)(\bar{b}\bar{s})^*$	9	[4; 3]	15141	15120
K_1	10	[7; 5]	15129	
	11	[8; 5]	15091	
	12	[9; 5]	15111	
	13	[7; 6]	15094	
	14	[8; 6]	15127	
	15	[9; 6]	15077	15008
K_2	16	[10; 7]	15073	
	17	[11; 7]	15042	
	18	[12; 7]	15024	
	19	[10; 8]	15103	
	20	[11; 8]	15131	
	21	[12; 8]	15119	15005
K_3	22	[13; 10]	15138	
	23	[14; 10]	15147	
	24	[15; 9]	15111	15106
K_4	25	[16; 11]	15156	
	26	[17; 11]	15169	
	27	[18; 11]	15497	
	28	[16; 12]	15157	
	29	[17; 12]	15156	
	30	[18; 12]	15142	15068
K_5	31	[19; 14]	15155	
	32	[20; 14]	15152	
	33	[21; 13]	15101	15098
Complete coupled-channels:				14854

ticular, the higher resonance is consistent with the result in Ref. [36].

Some properties of these two resonance states are summarized in Table XXVII. Particularly, their magnetic

TABLE XXV. Compositeness of exotic resonances obtained in a complete coupled-channel calculation in the $0(1^+)$ state of $\bar{b}b\bar{s}b$ tetraquark. Results are similarly organized as those in Table V.

Resonance	Structure
15440 - $i2.6$	$\mu = 0.382$ $r_{b\bar{b}} : 1.01; r_{\bar{b}s} : 1.49; r_{b\bar{s}} : 1.19; r_{bb} : 1.39$
Set I:	$S : 2.3\%; H : 2.5\%; Di : 2.2\%; K : 93.0\%$
Set II:	$S : 10.1\%; H : 3.8\%; Di : 5.0\%; K : 81.1\%$
15531 - $i0.4$	$\mu = 0.496$ $r_{b\bar{b}} : 1.01; r_{\bar{b}s} : 1.48; r_{b\bar{s}} : 1.20; r_{bb} : 1.37$
Set I:	$S : 0.8\%; H : 2.3\%; Di : 1.7\%; K : 95.2\%$
Set II:	$S : 2.8\%; H : 2.9\%; Di : 3.0\%; K : 91.3\%$
15632 - $i3.2$	$\mu = 0.355$ $r_{b\bar{b}} : 0.83; r_{\bar{b}s} : 1.22; r_{b\bar{s}} : 1.02; r_{bb} : 1.07$
Set I:	$S : 1.5\%; H : 1.8\%; Di : 3.0\%; K : 93.7\%$
Set II:	$S : 8.9\%; H : 7.1\%; Di : 5.3\%; K : 78.7\%$
15653 - $i6.3$	$\mu = 0.226$ $r_{b\bar{b}} : 0.89; r_{\bar{b}s} : 1.28; r_{b\bar{s}} : 1.09; r_{bb} : 1.03$
Set I:	$S : 1.7\%; H : 1.1\%; Di : 3.3\%; K : 93.9\%$
Set II:	$S : 8.9\%; H : 2.7\%; Di : 6.2\%; K : 82.2\%$

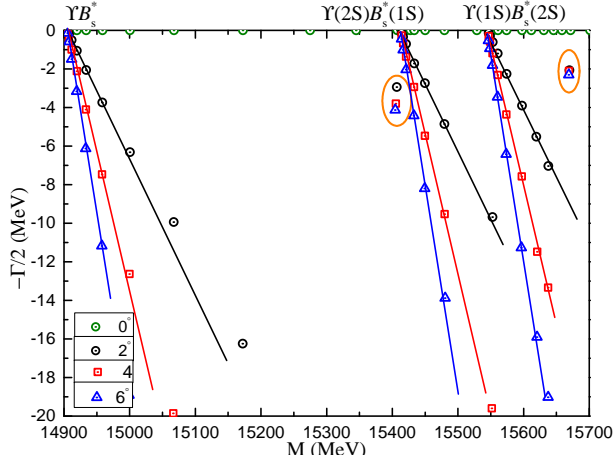


FIG. 13. The complete coupled-channels calculation of $\bar{b}b\bar{s}b$ tetraquark system with $I(J^P) = 0(2^+)$ quantum numbers.

moments are both $0.503\mu_N$. Besides, the first resonance has a size of ~ 0.7 fm and the other state is a little larger with size of $1.0-1.5$ fm. The dominant component, which is more than 80%, comes from K-type channels for these two resonances.

TABLE XXVI. Lowest-lying $\bar{b}b\bar{s}b$ tetraquark states with $I(J^P) = 0(2^+)$ calculated within the real range formulation of the chiral quark model. Results are similarly organized as those in Table IV (unit: MeV).

Channel	Index	$\chi_{J^i}^{\sigma_i}; \chi_j^c$ [$i; j$]	M	Mixed
$(\Upsilon B_s^*)^1(14875)$	1	[1; 1]	14905	
$(\Upsilon B_s^*)^8$	2	[1; 3]	15127	
$(bb)^*(\bar{b}\bar{s})^*$	3	[1; 7]	15161	
K_1	4	[1; 8]	15112	
	5	[1; 10]	15137	15055
K_2	6	[1; 11]	15086	
	7	[1; 12]	15119	15076
K_3	8	[1; 14]	15155	
K_4	9	[1; 8]	15500	
	10	[1; 10]	15162	15121
K_5	11	[1; 11]	15166	
Complete coupled-channels:				14905

TABLE XXVII. Compositeness of exotic resonances obtained in a complete coupled-channel calculation in the $0(2^+)$ state of $\bar{b}b\bar{s}b$ tetraquark. Results are similarly organized as those in Table V.

Resonance	Structure
15405 - $i7.6$	$\mu = 0.503$ $r_{b\bar{b}} : 0.68; r_{\bar{b}s} : 0.89; r_{b\bar{s}} : 0.74; r_{bb} : 0.71$
Set I:	$S : 0.6\%; H : 0.7\%; Di : 2.3\%; K : 96.4\%$
Set II:	$S : 4.5\%; H : 6.4\%; Di : 6.5\%; K : 82.6\%$
15669 - $i4.2$	$\mu = 0.503$ $r_{b\bar{b}} : 0.99; r_{\bar{b}s} : 1.56; r_{b\bar{s}} : 1.31; r_{bb} : 1.35$
Set I:	$S : 0.6\%; H : 1.1\%; Di : 1.9\%; K : 96.4\%$
Set II:	$S : 3.8\%; H : 3.7\%; Di : 4.5\%; K : 88.0\%$

IV. SUMMARY

Triply heavy tetraquarks, $\bar{Q}Q\bar{q}Q$ ($q = u, d, s; Q = c, b$), with spin-parity $J^P = 0^+, 1^+$ and 2^+ , and isospin 0 and $\frac{1}{2}$, have been systematically investigated within a constituent quark model framework which has been widely used in heavy quark sectors. Moreover, meson-meson, diquark-antidiquark and K-type arrangements are comprehensively considered, taking into account all corresponding color, spin and flavor configurations. Furthermore, a highly accurate and efficient

numerical method, dealing simultaneously with bound, resonant and scattering states, is employed to solve the 4-body Schrödinger-like equation. For each $I(J^P)$ case, single channel calculation is performed firstly, whereas partially and fully coupled-channel computations are developed later. In the last case, narrow resonances are obtained in each $I(J^P)$ case.

Our findings for $\bar{c}c\bar{q}q$ and $\bar{b}b\bar{q}q$ tetraquarks are summarized in Table XXVIII. In particular, complex mass, average size and magnetic moment of resonances are collected according to the quantum numbers $I(J^P)$, which are shown in the first column; the second column is about the resonance's pole position, and the third one shows average size and magnetic moment.

Some conclusions can be highlighted. Firstly, several narrow resonances with widths less than 11 MeV are found within an energy region 5.6 – 5.9 GeV and 15.3 – 15.7 GeV for triply charm and bottom tetraquarks, respectively. Secondly, the magnetic moment of 0^+ states is zero for both charm and bottom cases; meanwhile, it is negative valued for 1^+ and 2^+ states with $I = \frac{1}{2}$, but

positive for the isoscalar cases. Thirdly, the average size of those resonances obtained in the $\bar{b}b\bar{q}q$ tetraquark sector is less than 1.8 fm, except for the $I(J^P) = 0(0^+)$ $\bar{b}b\bar{d}b$ tetraquark with a size of 1.5 – 2.2 fm. In the case of $\bar{c}c\bar{q}q$ tetraquarks, one can find compact and loosely bound molecules. Finally, the dominant component of all these resonances is usually of K-type configuration.

ACKNOWLEDGMENTS

Work partially financed by National Natural Science Foundation of China under Grant Nos. 12305093, 11535005 and 11775118; Zhejiang Provincial Natural Science Foundation under Grant No. LQ22A050004; Ministerio Español de Ciencia e Innovación under grant No. PID2022-140440NB-C22; Junta de Andalucía under contract Nos. PAIDI FQM-370 and PCI+D+i under the title: "Tecnologías avanzadas para la exploración del universo y sus componentes" (Code AST22-0001).

-
- [1] R. Aaij *et al.* (LHCb), *Phys. Rev. D* **102**, 112003 (2020), arXiv:2009.00026 [hep-ex].
- [2] R. Aaij *et al.* (LHCb), *Phys. Rev. Lett.* **125**, 242001 (2020), arXiv:2009.00025 [hep-ex].
- [3] R. Aaij *et al.* (LHCb), *Phys. Rev. Lett.* **131**, 041902 (2023), arXiv:2212.02716 [hep-ex].
- [4] R. Aaij *et al.* (LHCb), *Phys. Rev. D* **108**, 012017 (2023), arXiv:2212.02717 [hep-ex].
- [5] R. Aaij *et al.* (LHCb), *Nature Phys.* **18**, 751 (2022), arXiv:2109.01038 [hep-ex].
- [6] R. Aaij *et al.* (LHCb), *Nature Commun.* **13**, 3351 (2022), arXiv:2109.01056 [hep-ex].
- [7] R. Aaij *et al.* (LHCb), *Sci. Bull.* **65**, 1983 (2020), arXiv:2006.16957 [hep-ex].
- [8] A. Hayrapetyan *et al.* (CMS), *Phys. Rev. Lett.* **132**, 111901 (2024), arXiv:2306.07164 [hep-ex].
- [9] G. Aad *et al.* (ATLAS), *Phys. Rev. Lett.* **131**, 151902 (2023), arXiv:2304.08962 [hep-ex].
- [10] X.-K. Dong, F.-K. Guo, and B.-S. Zou, *Phys. Rev. Lett.* **126**, 152001 (2021), arXiv:2011.14517 [hep-ph].
- [11] H.-X. Chen, W. Chen, X. Liu, and S.-L. Zhu, *Phys. Rept.* **639**, 1 (2016), arXiv:1601.02092 [hep-ph].
- [12] H.-X. Chen, W. Chen, X. Liu, Y.-R. Liu, and S.-L. Zhu, *Rept. Prog. Phys.* **80**, 076201 (2017), arXiv:1609.08928 [hep-ph].
- [13] F.-K. Guo, C. Hanhart, U.-G. Meißner, Q. Wang, Q. Zhao, and B.-S. Zou, *Rev. Mod. Phys.* **90**, 015004 (2018), arXiv:1705.00141 [hep-ph].
- [14] Y.-R. Liu, H.-X. Chen, W. Chen, X. Liu, and S.-L. Zhu, *Prog. Part. Nucl. Phys.* **107**, 237 (2019), arXiv:1903.11976 [hep-ph].
- [15] G. Yang, J. Ping, and J. Segovia, *Symmetry* **12**, 1869 (2020), arXiv:2009.00238 [hep-ph].
- [16] X.-K. Dong, F.-K. Guo, and B.-S. Zou, *Commun. Theor. Phys.* **73**, 125201 (2021), arXiv:2108.02673 [hep-ph].
- [17] H.-X. Chen, *Phys. Rev. D* **105**, 094003 (2022), arXiv:2103.08586 [hep-ph].
- [18] X. Cao, (2023), arXiv:2301.11253 [hep-ph].
- [19] M. Mai, U.-G. Meißner, and C. Urbach, *Phys. Rept.* **1001**, 1 (2023), arXiv:2206.01477 [hep-ph].
- [20] L. Meng, B. Wang, G.-J. Wang, and S.-L. Zhu, (2022), arXiv:2204.08716 [hep-ph].
- [21] H.-X. Chen, W. Chen, X. Liu, Y.-R. Liu, and S.-L. Zhu, *Rept. Prog. Phys.* **86**, 026201 (2023), arXiv:2204.02649 [hep-ph].
- [22] F.-K. Guo, H. Peng, J.-J. Xie, and X. Zhou, (2022), arXiv:2203.07141 [hep-ph].
- [23] P. G. Ortega and D. R. Entem, *Symmetry* **13**, 279 (2021), arXiv:2012.10105 [hep-ph].
- [24] H. Huang, C. Deng, X. Liu, Y. Tan, and J. Ping, *Symmetry* **15**, 1298 (2023).
- [25] R. F. Lebed, *PoS FPCP2023*, 028 (2023), arXiv:2308.00781 [hep-ph].
- [26] B.-S. Zou, *Sci. Bull.* **66**, 1258 (2021), arXiv:2103.15273 [hep-ph].
- [27] M.-L. Du, V. Baru, F.-K. Guo, C. Hanhart, U.-G. Meißner, J. A. Oller, and Q. Wang, *JHEP* **08**, 157 (2021), arXiv:2102.07159 [hep-ph].
- [28] M.-Z. Liu, Y.-W. Pan, Z.-W. Liu, T.-W. Wu, J.-X. Lu, and L.-S. Geng, (2024), arXiv:2404.06399 [hep-ph].
- [29] D. Johnson, I. Polyakov, T. Skwarnicki, and M. Wang, (2024), 10.1146/annurev-nucl-102422-040628, arXiv:2403.04051 [hep-ex].
- [30] Z.-H. Zhu, W.-X. Zhang, and D. Jia, *Eur. Phys. J. C* **84**, 344 (2024), arXiv:2312.01908 [hep-ph].
- [31] Y. Liu, M. A. Nowak, and I. Zahed, *Phys. Rev. D* **100**, 126023 (2019), arXiv:1904.05189 [hep-ph].
- [32] X.-Z. Weng, W.-Z. Deng, and S.-L. Zhu, *Phys. Rev. D* **105**, 034026 (2022), arXiv:2109.05243 [hep-ph].
- [33] Q.-F. Lü, D.-Y. Chen, Y.-B. Dong, and E. Santopinto, *Phys. Rev. D* **104**, 054026 (2021), arXiv:2107.13930 [hep-ph].
- [34] J.-F. Jiang, W. Chen, and S.-L. Zhu, *Phys. Rev. D* **96**, 094022 (2017), arXiv:1708.00142 [hep-ph].

- [35] X. Liu, Y. Tan, D. Chen, H. Huang, and J. Ping, *Phys. Rev. D* **107**, 054019 (2023), arXiv:2205.08281 [hep-ph].
- [36] H. Mutuk, *Eur. Phys. J. C* **83**, 358 (2023), arXiv:2305.03358 [hep-ph].
- [37] Y. Xing, *Eur. Phys. J. C* **80**, 57 (2020), arXiv:1910.11593 [hep-ph].
- [38] K. Chen, X. Liu, J. Wu, Y.-R. Liu, and S.-L. Zhu, *Eur. Phys. J. A* **53**, 5 (2017), arXiv:1609.06117 [hep-ph].
- [39] G. Yang, J. L. Ping, and J. Segovia, *Phys. Rev. D* **101**, 014001 (2020).
- [40] G. Yang, J. Ping, and J. Segovia, *Phys. Rev. D* **102**, 054023 (2020).
- [41] G. Yang, J. Ping, and J. Segovia, *Phys. Rev. D* **104**, 014006 (2021), arXiv:2104.08814 [hep-ph].
- [42] G. Yang, J. Ping, and J. Segovia, *Eur. Phys. J. C* **83**, 772 (2023), arXiv:2303.15388 [hep-ph].
- [43] G. Yang, J. Ping, and J. Segovia, *Phys. Rev. D* **104**, 094035 (2021), arXiv:2109.04311 [hep-ph].
- [44] G. Yang, J. Ping, and J. Segovia, *Phys. Rev. D* **106**, 014021 (2022), arXiv:2204.08556 [hep-ph].
- [45] G. Yang, J. Ping, and J. Segovia, *Phys. Rev. D* **103**, 074011 (2021), arXiv:2101.04933 [hep-ph].
- [46] G. Yang, J. Ping, and J. Segovia, *Chin. Phys. C* **48**, 073106 (2024), arXiv:2311.10376 [hep-ph].
- [47] G. Yang, J. Ping, and F. Wang, *Phys. Rev. D* **95**, 014010 (2017).
- [48] G. Yang, J. Ping, and J. Segovia, *Phys. Rev. D* **99**, 014035 (2019), arXiv:1809.06193 [hep-ph].
- [49] G. Yang, J. L. Ping, and J. Segovia, *Phys. Rev. D* **101**, 074030 (2020).
- [50] G. Yang, J. Ping, and J. Segovia, *Phys. Rev. D* **106**, 014005 (2022), arXiv:2205.11548 [hep-ph].
- [51] G. Yang, J. Ping, and J. Segovia, *Symmetry* **16**, 354 (2024), arXiv:2311.01044 [hep-ph].
- [52] E. Hiyama, Y. Kino, and M. Kamimura, *Prog. Part. Nucl. Phys.* **51**, 223 (2003).
- [53] G. S. Bali, H. Neff, T. Duessel, T. Lippert, and K. Schilling (SESAM), *Phys. Rev. D* **71**, 114513 (2005), arXiv:hep-lat/0505012 [hep-lat].
- [54] J. Vijande, F. Fernandez, and A. Valcarce, *J. Phys. G* **31**, 481 (2005), arXiv:hep-ph/0411299 [hep-ph].
- [55] J. Segovia, A. M. Yasser, D. R. Entem, and F. Fernandez, *Phys. Rev. D* **78**, 114033 (2008).
- [56] J. Segovia, D. R. Entem, and F. Fernandez, *Phys. Rev. D* **91**, 094020 (2015), arXiv:1502.03827 [hep-ph].
- [57] J. Segovia, P. G. Ortega, D. R. Entem, and F. Fernández, *Phys. Rev. D* **93**, 074027 (2016), arXiv:1601.05093 [hep-ph].
- [58] G. Yang, J. Ping, P. G. Ortega, and J. Segovia, *Chin. Phys. C* **44**, 023102 (2020), arXiv:1904.10166 [hep-ph].
- [59] P. G. Ortega, J. Segovia, D. R. Entem, and F. Fernandez, *Eur. Phys. J. C* **80**, 223 (2020), arXiv:2001.08093 [hep-ph].
- [60] J. Segovia, D. R. Entem, and F. Fernandez, *Phys. Rev. D* **83**, 114018 (2011).
- [61] J. Segovia, C. Albertus, D. R. Entem, F. Fernandez, E. Hernandez, and M. A. Perez-Garcia, *Phys. Rev. D* **84**, 094029 (2011), arXiv:1107.4248 [hep-ph].
- [62] J. Segovia, D. R. Entem, and F. Fernández, *Phys. Rev. D* **91**, 014002 (2015), arXiv:1409.7079 [hep-ph].
- [63] B. Martín-González, P. G. Ortega, D. R. Entem, F. Fernández, and J. Segovia, *Phys. Rev. D* **106**, 054009 (2022), arXiv:2205.05950 [hep-ph].
- [64] P. G. Ortega, J. Segovia, D. R. Entem, and F. Fernández, *Phys. Rev. D* **95**, 034010 (2017), arXiv:1612.04826 [hep-ph].
- [65] P. G. Ortega, J. Segovia, D. R. Entem, and F. Fernández, *Eur. Phys. J. C* **79**, 78 (2019), arXiv:1808.00914 [hep-ph].
- [66] P. G. Ortega, J. Segovia, and F. Fernandez, *Phys. Rev. D* **104**, 094004 (2021), arXiv:2107.02544 [hep-ph].
- [67] P. G. Ortega, J. Segovia, D. R. Entem, and F. Fernandez, *Phys. Lett. B* **827**, 136998 (2022), arXiv:2111.00023 [hep-ph].
- [68] J. Segovia, D. R. Entem, F. Fernandez, and E. Hernandez, *Int. J. Mod. Phys. E* **22**, 1330026 (2013), arXiv:1309.6926 [hep-ph].

TABLE XXVIII. Summary of resonance structures found in the $\bar{Q}Q\bar{q}q$ ($q = u, d, s$; $Q = c, b$) tetraquark systems. The first column shows the isospin, total spin and parity of each singularity. The second column refers to the theoretical resonance with notation: $E = M - i\Gamma$ (unit: MeV). Size (r , unit: fm) and magnetic moment (μ , unit: μ_N) of resonance are presented in the last column.

$I(J^P)$	Theoretical resonance $E = M - i\Gamma$	Structure r, μ
$\bar{c}c\bar{q}q$ tetraquarks		
$\frac{1}{2}(0^+)$	5592 - $i2.5$	0.95 ~ 1.45, 0
	5714 - $i1.8$	1.30 ~ 1.90, 0
	5828 - $i2.6$	1.30 ~ 1.85, 0
$\frac{1}{2}(1^+)$	5693 - $i3.0$	1.25 ~ 1.75, -1.06
$\frac{1}{2}(2^+)$	5691 - $i5.9$	0.90 ~ 1.20, -1.64
	5827 - $i2.3$	1.25 ~ 1.80, -1.64
$0(0^+)$	5682 - $i4.6$	1.50 ~ 2.10, 0
	5855 - $i2.8$	1.05 ~ 1.40, 0
$0(1^+)$	5863 - $i6.6$	1.60 ~ 2.30, 0.578
	5941 - $i1.8$	1.15 ~ 1.55, 0.503
	5942 - $i5.6$	1.30 ~ 1.95, 0.068
$0(2^+)$	5788 - $i3.1$	0.80 ~ 1.10, 0.921
	5943 - $i5.1$	1.40 ~ 2.05, 0.921
$\bar{b}b\bar{q}q$ tetraquarks		
$\frac{1}{2}(0^+)$	15320 - $i0.5$	0.95 ~ 1.55, 0
	15331 - $i4.5$	1.20 ~ 1.80, 0
	15372 - $i6.1$	1.10 ~ 1.70, 0
	15407 - $i9.3$	1.05 ~ 1.60, 0
$\frac{1}{2}(1^+)$	15327 - $i1.5$	1.05 ~ 1.60, -1.453
	15376 - $i3.2$	1.00 ~ 1.65, -1.817
	15395 - $i4.2$	0.95 ~ 1.50, -1.456
	15417 - $i10.2$	0.95 ~ 1.50, -1.771
$\frac{1}{2}(2^+)$	15308 - $i9.3$	0.60 ~ 0.95, -2.061
	15449 - $i1.4$	0.75 ~ 1.30, -2.061
	15558 - $i5.4$	1.00 ~ 1.55, -2.061
$0(0^+)$	15381 - $i2.0$	0.65 ~ 1.10, 0
	15439 - $i2.6$	1.50 ~ 2.20, 0
	15464 - $i6.2$	1.30 ~ 1.90, 0
	15531 - $i0.8$	0.85 ~ 1.35, 0
$0(1^+)$	15440 - $i2.6$	1.00 ~ 1.50, 0.382
	15531 - $i0.4$	1.00 ~ 1.50, 0.496
	15632 - $i3.2$	0.80 ~ 1.25, 0.355
	15653 - $i6.3$	0.85 ~ 1.30, 0.226
$0(2^+)$	15405 - $i7.6$	0.65 ~ 0.90, 0.503
	15669 - $i4.2$	0.95 ~ 1.60, 0.503